UNIVERSITAT DE BARCELONA

Departament d'Astronomia i Meteorologia


# Astrophysical Studies on Open Clusters:

## NGC 1807, NGC 1817, NGC 2548 and NGC 2682

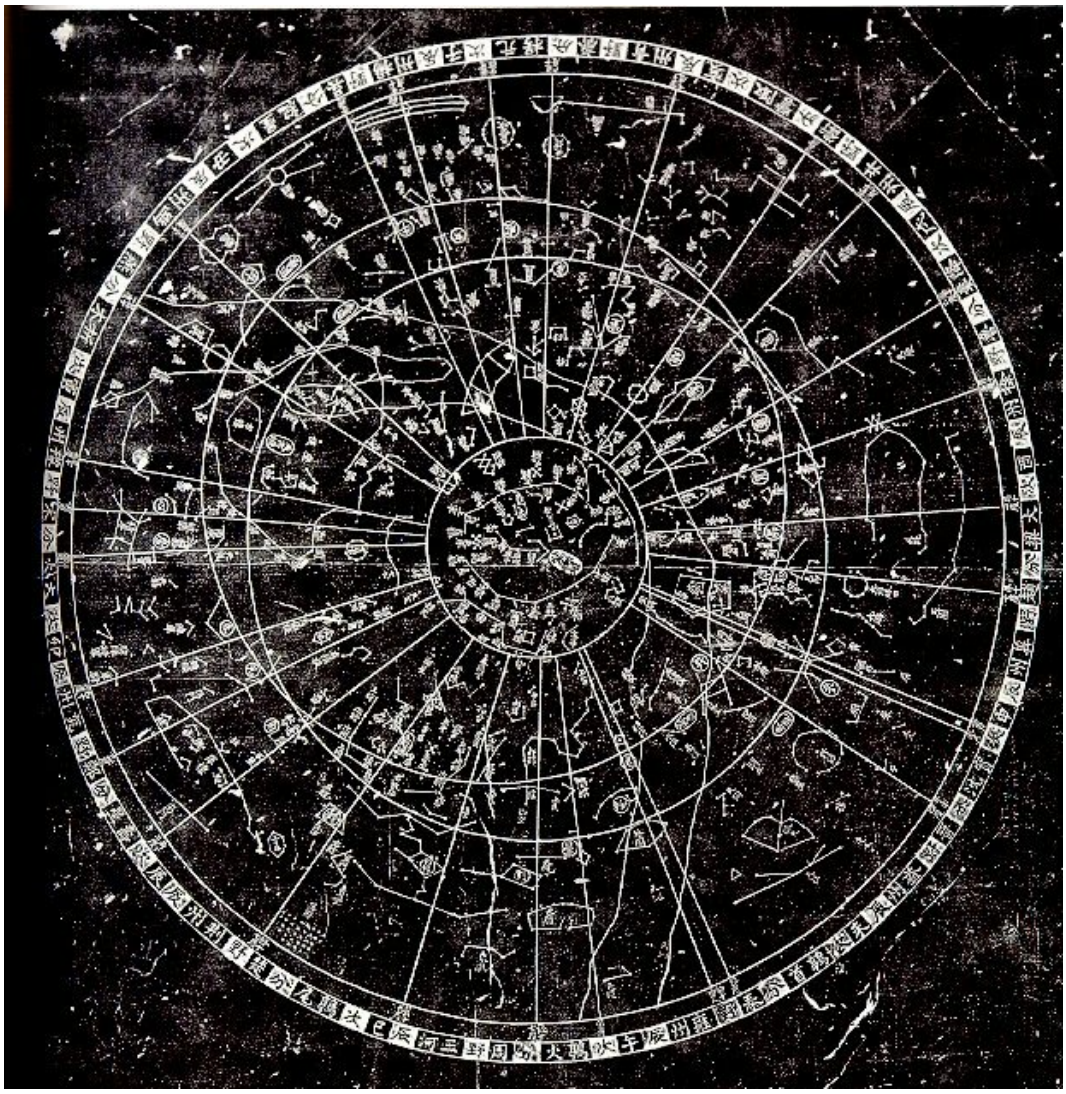

Memoria presentada por

**María de los Dolores Balaguer Núñez**

para optar al grado de

Doctora en Física

Barcelona, 31 de octubre de 2005

## 嫦 娥

云母屏风烛影深，
长河渐落晓星沈。
嫦娥应悔偷灵药，
碧海青天夜夜心。

李 商 隐 (812-858)

**The Lady in the Moon**[a]

Behind the mica screen, in shadows deep, a candle flickers,
The Milky Way has faded, and the morning star declines.
Chang E[b] must regret having stolen the magic elixir —
In that blue ocean of a sky: endless thoughts, night after night.

Li Shangyin (c. 812 - 858)

[a] Translated by Wilson & Zhang (1995)
[b] Denizen of the moon that stole the elixir of inmortality

# 7 NGC 2548, NGC 1817 and NGC 2682: Physical analysis

In the previous chapters, deep astrometric and photometric analysis of the open clusters NGC 2548 (M 48), NGC 1817 and NGC 2682 (M 67) have been performed. We have a set of three clusters with a sequence of ages (0.4, 1.1 and 4.2 Gyr) and metallicities ($-0.34$,$-0.24$ and $+0.01$). From a list of candidate member stars (up to the limit of our photometry) for each of the clusters as well as a determination of their basic physical parameters, we are now able to deepen the study and compare more general characteristics.

In this chapter, from the kinematical data of the clusters, we calculate their space velocity and Galactic orbital parameters. The knowledge of their space velocity and Galactic orbit is fundamental for a deeper understanding of the dynamical processes involved. The relation of these orbital parameters with the metallicity gives also one more brick in the analysis of an age/distance metallicity relation.

We use the obtained fundamental parameters to determine the luminosity and mass functions of the three clusters, as well as their mass function slopes. The relaxation time, degree of mass segregation and surface brightness of their different types of stars offer us an insight of their evolutionary stage.

Blue straggler stars are found in all populations: in the field, in open clusters of all ages (Population I, young disk, old disk), in globular clusters (Population II, halo), and in dwarf galaxies. Whether they are single stars or binaries, they signal a still incomplete understanding of stellar evolution and also of star formation within clusters. Moreover, they exist in significant numbers in young and old populations and it is therefore important to gather information on their nature if we wish to correctly characterise stellar populations in other galaxies.

Gaps in the colour-magnitude diagram of clusters have also been a subject of debate. We make use of our photometry to get the effective temperature distribution along the main sequence of the clusters to find several gaps. A test to study the significance of these gaps in the main sequence is applied and the method is also extended to Hyades and Pleiades to construct a sequence of ages and metallicities.

## 7.1 Space velocity and Galactic orbit

By combining our absolute proper motions with radial velocities from the literature, and the age and distance calculated in previous chapters, we determine the space velocity and the Galactic orbit of each of the clusters under study. We use the model developed by Asiain (1998) and Asiain et al. (1999). The model consists in a realistic estimation of the Galactic gravitational potential with three components: the general axisymetric potential (Allen & Santillan 1991), the spiral arms (Lin & Shu 1964; Lin et al. 1969) and a central bar (Palouš et al. 1993). We also adopted the updated values of the parameters by Fernández (2005) for two models: one with four spiral arms and a pitch angle of 14.°0 and one with two arms and a pitch angle of 6.°0.

To obtain the velocity of the cluster in the Galactocentric frame, we assumed the motion of the Sun in the LSR to be $(U, V, W)_{\odot} = (10.00, 5.25, 7.17)$ km s$^{-1}$ (Dehnen & Binney 1998), where the $U$ is defined pointing to the centre of the Galaxy, the $V$ is directed towards the direction of the Galactic rotation and $W$ towards te North Galactic pole. Following Asiain (1998), the Galactocentric coordinates $(X, Y, Z)$ are taken as defined in the Figure 7.1. For present time ($t = 0$), the $Y$-axis direction coincides with the Sun-Galactic centre direction. We adopted the current IAU standard values of $\Theta_{\odot} = 220$ km s$^{-1}$ for the local circular rotation velocity and

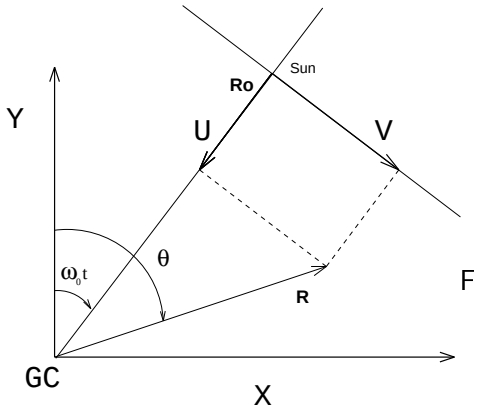


Figure 7.1: Definition of heliocentric and Galactocentric coordinate systems. Figure taken from Asiain (1998).

Table 7.1: Present Kinematic Data

| Cluster | $\mu_\alpha \cos\delta$ mas yr$^{-1}$ | $\mu_\delta$ mas yr$^{-1}$ | $V_{\rm rad}$ km s$^{-1}$ | $(X, Y, Z)$ kpc | $(U, V, W)$ km s$^{-1}$ |
|---|---|---|---|---|---|
| NGC 2548 | $-1.10$ | 2.09 | $+8.90$[a] | $(-0.52, 8.97, +0.19)$ | $(-11.7, -0.8, 2.7)$ |
| NGC 1817 | 0.29 | $-0.96$ | $+65.33$[b] | $(-0.19, 10.23, -0.41)$ | $(-61.8, -14.8, -17.3)$ |
| NGC 2682 | $-7.10$ | $-7.60$ | $+33.44$[c] | $(-0.45, 9.12, +0.48)$ | $(-31.2, -42.1, -16.9)$ |

(a) Wallerstein et al. (1963); (b) Mermilliod et al. (2003); (c) Mathieu et al. (1986, 1990)

$R_\odot = 8.5$ kpc for the Sun Galactocentric distance, and the updated value of $\omega_0 = 25.8498$ km s$^{-1}$ kpc$^{-1}$ (Fernández 2005). The resulting Galactocentric position and velocity of each cluster as well as the kinematic data used are given in Table 7.1.

These vectors, together with the Galactic gravitational potential model and the cluster ages ($t = 0.4$, 1.1, 4.2 Gyr) determine the orbit of each cluster in the Galaxy. The resulting orbits are characterised by the orbital parameters given in Table 7.2. Pericentric, $R_{\rm p}$, and apocentric, $R_{\rm a}$, radii are determined from the minimum and maximum of $(R^2 + z^2)^{1/2}$ averaged over the number of cycles. Similarly, the maximum distance above (or below) the plane, $z_{\rm max}$ ($z_{\rm min}$), is an average over the number of plane crossings. The inclination angle with respect to the Galactic plane is defined as $\Psi = \sin^{-1}(z_{\rm maxim}/r_{z_{\rm maxim}})$, where $z_{\rm maxim}$ is the largest absolute value of $z_{\rm min}$ and $z_{\rm max}$, and $r_{z_{\rm maxim}}$ is $(R^2 + z^2)^{1/2}$ at $z_{\rm maxim}$, and the angle is averaged over the number of plane crossings. Eccentricities are calculated as $e = (R_{\rm a} - R_{\rm p})/(R_{\rm a} + R_{\rm p})$. where $R_{\rm a}$ and $R_{\rm p}$ are averages. The uncertainty estimates in the averaged orbital parameters are the dispersions over the number of cycles, while for the eccentricity the uncertainty is propagated from the dispersions of $R_{\rm a}$ and $R_{\rm p}$. The orbits of the three clusters for the four spiral arms model are shown in Figure 7.2 and 7.3. The panels on the left show the orbit projected onto the disk plane of the Galaxy, while the panels on the right show the orbit onto the plane perpendicular to the Galatic disk and containing the Sun.

The differences between four and two arms models are inside the quoted intrinsic dispersions (see Table 7.2), which are due to the dinamics of the clusters under the potential. Moreover, these differences are below the uncertainties of proper motions and distance, which are the dominant source of error in the orbital parameters, as already pointed by Dinescu et al. (1999).

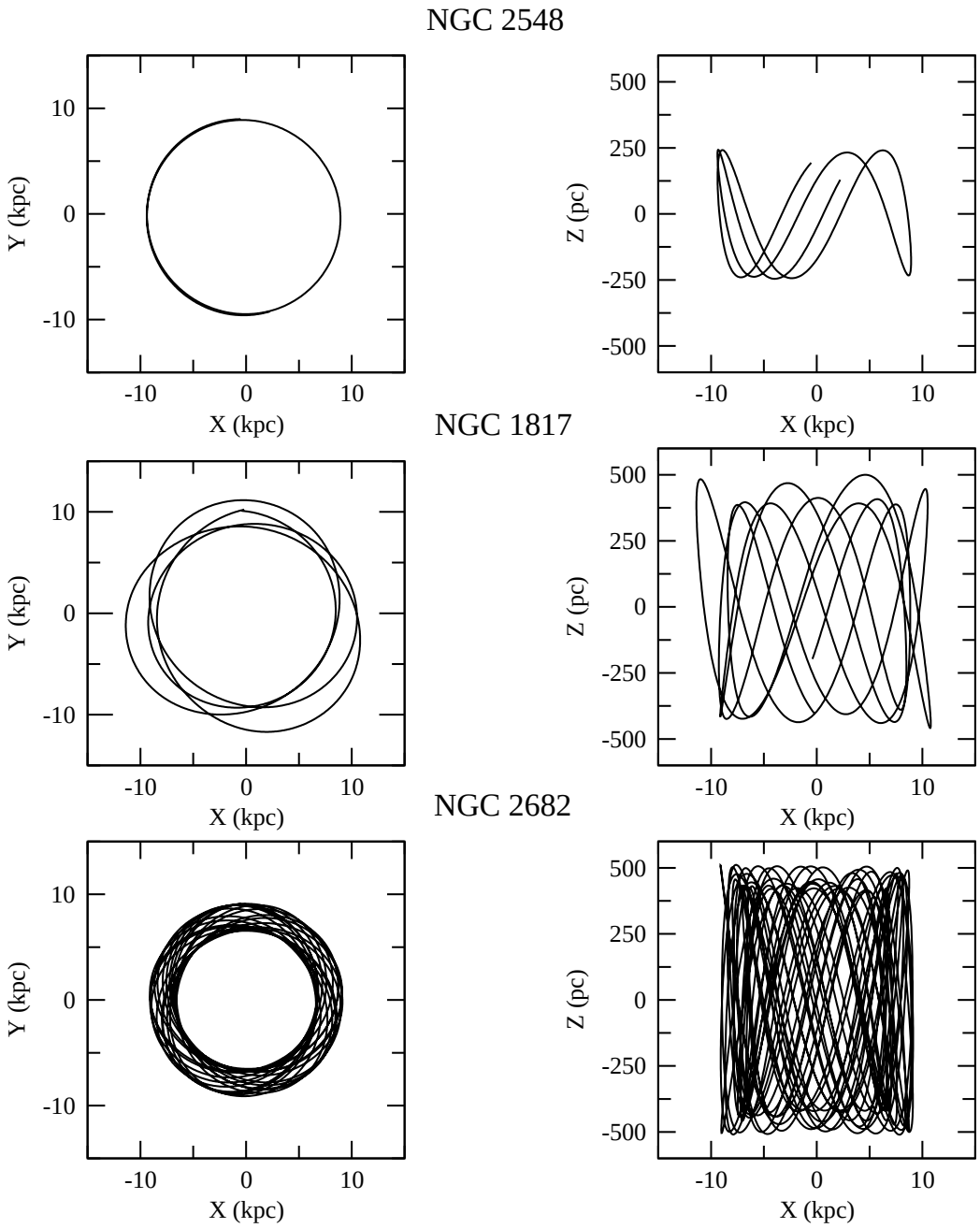


Figure 7.2: The orbits of the three clusters under study: NGC 2548 (M 48), NGC 1817 and NGC 2682 (M 67), calculated with the model with four spiral arms. The panels on the left show the orbit projected on the disk plane of the Galaxy, while the panels on the right show the orbit projected on the plane perpendicular to the Galactic disk and containing the Sun.

Table 7.2: Orbital parameters for the clusters under study.

| Cluster & model | $R_a$ kpc | $R_p$ kpc | $e$ | $z_{max}$ pc | $z_{min}$ pc | Rev. | Cross. | $\Psi$ deg |
|---|---|---|---|---|---|---|---|---|
| NGC 2548 | | | | | | | | |
| Four arms | 9.56±0.07 | 8.73±0.00* | 0.045±0.000 | 239.4±2.3 | −240.1±2.2 | 1.53 | 10 | 1.48±0.01 |
| Two arms | 9.41±0.11 | 9.01±0.14 | 0.022±0.000 | 239.3±2.1 | −239.5±1.3 | 1.53 | 10 | 1.48±0.00 |
| NGC 1817 | | | | | | | | |
| Four arms | 10.92±0.40 | 8.48±0.03 | 0.126±0.013 | 424.8±12.7 | −424.5±6.1 | 5.00 | 22 | 2.47±0.02 |
| Two arms | 11.41±0.60 | 8.46±0.02 | 0.149±0.027 | 438.4±15.4 | −434.1±9.6 | 5.83 | 20 | 2.40±0.02 |
| NGC 2682 | | | | | | | | |
| Four arms | 9.13±0.01 | 6.61±0.01 | 0.160±0.001 | 461.4±4.6 | −461.5±4.7 | 26.81 | 100 | 3.28±0.01 |
| Two arms | 9.09±0.01 | 6.63±0.01 | 0.156±0.001 | 458.0±4.4 | −459.5±4.7 | 21.85 | 100 | 3.26±0.01 |

(*) Only one pericentre passage has occurred during the cluster's lifetime.

We can also notice that for our three clusters, the eccentricities grow with age, being NGC 2682 the one with the most eccentric orbit. Age could be also related with the inclination angle with respect to the Galactic plane.

As explained in Asiain (1998), the description and classification of three-dimensional orbits in an axisymmetric potential can be performed by means of the meridional plane $Z$ vs $R$. Our orbits fill a tube with a hole around the symmetry axis (the shortest Galactic axis), like a doughnut. These orbits are called short-axis tube orbits and can be classified in different types, from periodic to stochastic or irregular orbits. The dispersions in the radii are indicative of the intrinsic nature of the orbit, and this may be due to effects such as chaos as described by Schuster & Allen (1997). In our set, we can notice the biggest dispersion in the orbit of NGC 1817, clearly shown in Figure 7.3, where all the orbits have been integrated during the same interval of 10 Gyr.

We currently observe the clusters near their maximum distance from the plane. This is consistent with the expectation of a higher probability of finding clusters near their maximum $|z|$, where the clusters spend more time due to their vertical motion. The scale height of old open clusters, 375 pc (Janes & Phelps 1994), is slightly larger than that of the old disk, which shows scale heights of 250 pc for the giants and 325 pc for the late-type dwarfs (Yoshii et al. 1987). The selective destruction of clusters close to the plane has left behind old clusters that share the general disk rotation but have larger scale heights compared with most disk objects of similar age. Clusters with kinematics that keep them away from the disk or the

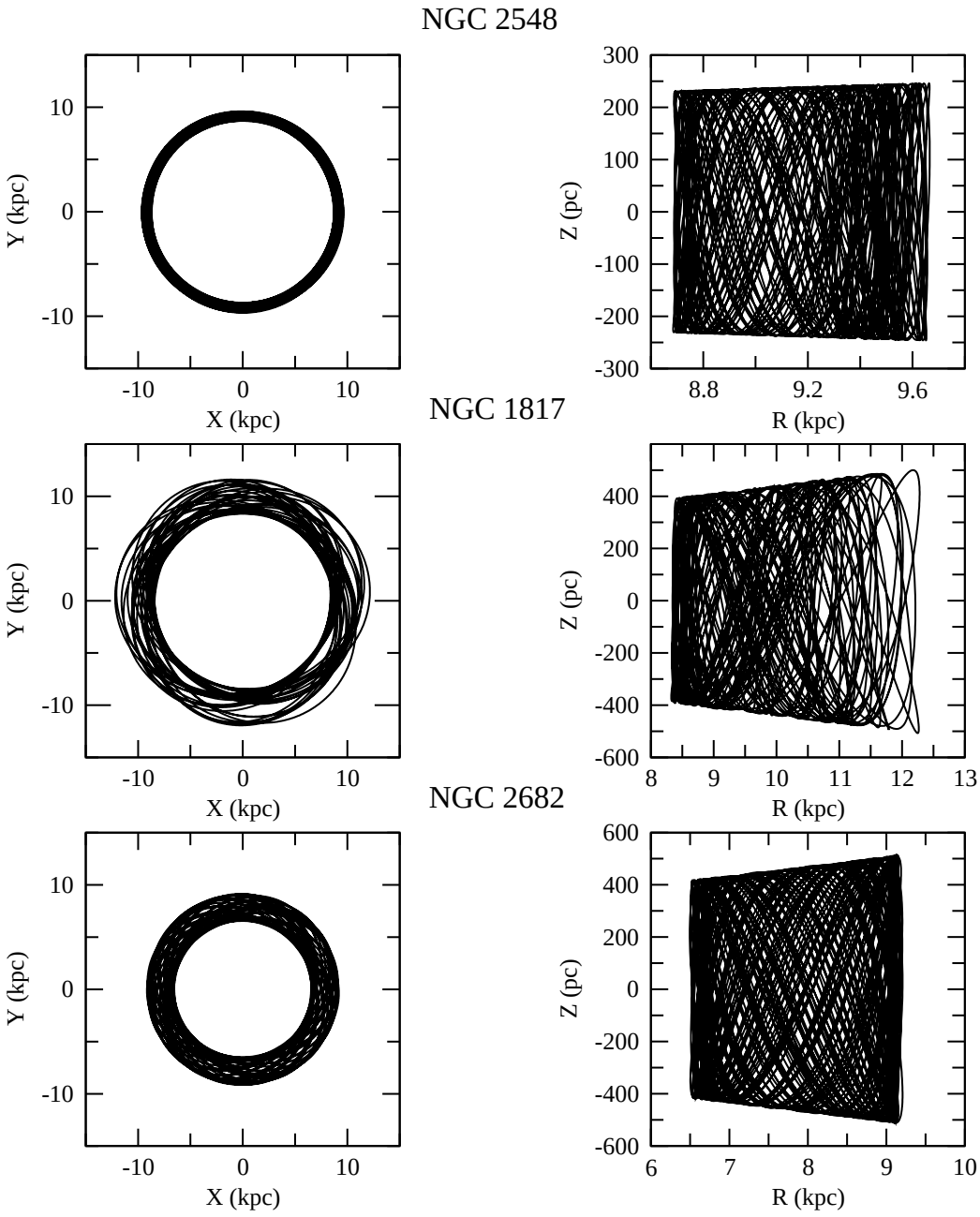


Figure 7.3: The orbits of the three clusters under study: NGC 2548 (M 48), NGC 1817 and NGC 2682 (M 67), calculated with the model with four spiral arms for an integration time equal for the three clusters and of 10 Gyr. The panels on the left show the orbit projected on the disk plane of the Galaxy, while the panels on the right show $Z$ vs $R$.

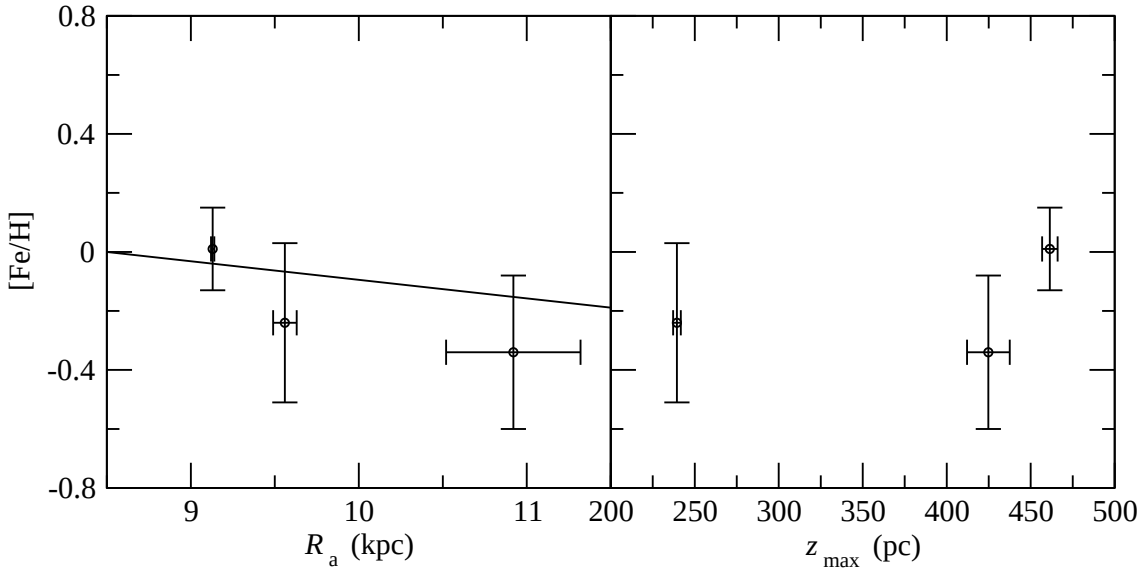


Figure 7.4: The metallicity (-0.34,-0.24,+0.01) for NGC 1817, NGC 2548 (M 48), and NGC 2682 (M 67) respectively, vs the apogalactic radius, $R_{\rm a}$, on the left panel and the maximum distance above the plane $z_{\rm max}$ in the right panel. The solid line in the left panel is the gradient of $-0.063$ dex kpc$^{-1}$ found by Chen et al. (2003). No clear trend can be distinguished in the right panel.

inner regions of the Galaxy have been preferentially preserved. Their orbits lead to fewer interactions with giant molecular clouds, which are thought to be among the main factors in the disruption of open clusters.

The computed orbit for NGC 2548 predicts the last crossing at about 10 Myr ago. Bergond et al. (2001) derive this last disk shock between 20 and 40 Myr ago. Given the uncertainties in the orbital parameters both results agree qualitatively.

## 7.2 Age-metallicity relation

We have plotted the metallicity vs $R_{\rm a}$ and $z_{\rm max}$ for the three clusters in Figure 7.4. Chen et al. (2003) derived a metallicity radial gradient of $-0.063\pm0.008$ dex kpc$^{-1}$ from a sample of 119 open clusters, similar to the value of $-0.059\pm0.010$ dex kpc$^{-1}$ derived from the homogeneous sample by Friel et al. (2002). Another gradient result was presented by Carraro et al. (1998) from 37 selected clusters with spectroscopically obtained metallicities giving a gradient of $-0.09$ dex kpc$^{-1}$. In general, the

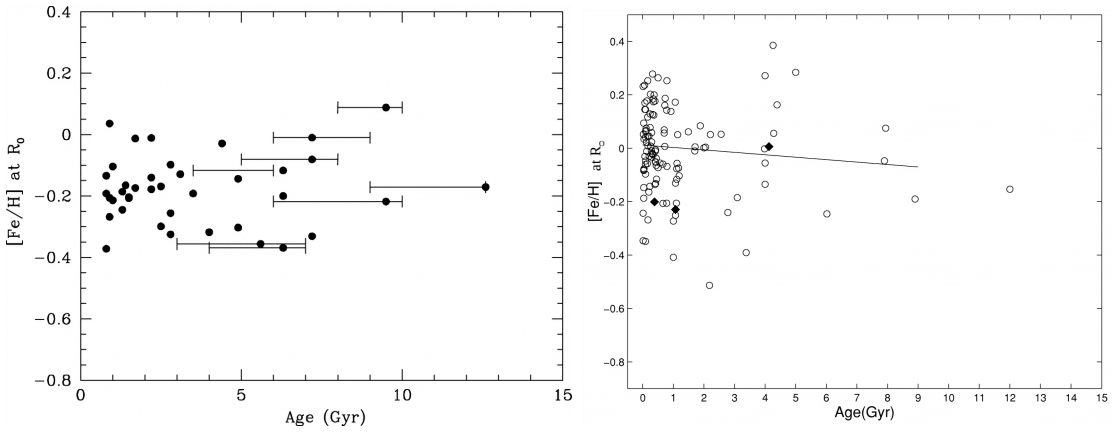


Figure 7.5: Left panel is Figure 4 from Friel et al. (2002) where age-metallicity relationship from their homogeneous sample of 39 old open clusters is shown. The age plotted is the relative age scale formed by the MAI from Janes & Phelps (1994). Horizontal bars show the maximum age range from values in the literature for the oldest clusters in the sample. Right panel is Figure 10 from Chen et al. (2003) with a larger sample of 118 clusters. The solid line is a least-square fit for their open cluster data. Metallicities in both cases have been corrected for the radial abundance gradient, assuming a uniform slope of -0.06 dex kpc$^{-1}$. Our results are overplotted as filled diamonds on this panel.

magnitude of the slope fit by a linear function has been found, in the literature, to be $-0.06$ to $-0.09$ dex kpc$^{-1}$, depending on the cluster sample and the metallicity determination. Our results are consistent with this range of gradients, as well as with the similar gradients obtained from other tracers, such as H II regions and planetary nebulae (see a summary in Hou et al. 2000). In any case, an intrinsic dispersion in [Fe/H] at any radial distance from the Galactic centre is expected.

The existence of a vertical metallicity gradient among old open clusters is controversial. Gilmore & Wyse (1985) showed that there is little or no gradient but a well-defined mean abundance in each component of the Galaxy. These components are identified as the Galactic thin disk, with a young ($\overline{[\mathrm{Fe/H}]} \simeq +0.00$ ($\sigma \simeq 0.15$) with exponential scale height $z_0 \simeq 100$ pc), and an old component ($\overline{[\mathrm{Fe/H}]} \simeq -0.3(0.2)$ with $z_0 \simeq 300$ pc), the thick disk ($\overline{[\mathrm{Fe/H}]} \simeq -0.6(0.3)$ and $z_0 \geq 1$ kpc) and the extreme spheroid ($\overline{[\mathrm{Fe/H}]} \simeq -1.5(0.5)$ and $z_0 \geq 4$ kpc). Friel (1995), Carraro & Chiosi (1994) and Salaris et al. (2004) studying open clusters do not find evidence for a vertical gradient either, whereas Chen et al. (2003) found a vertical abundance gradient of $-0.295 \pm 0.050$ dex kpc$^{-1}$ consistent with the results of Carraro et al.

(1998). But Carraro et al. constate that its existence and value are not firmly established, and it is likely caused by insufficient discrimination between different age groups. Our results are in agreement with a non-significant vertical abundance gradient (Figure 7.4 right).

It has been known for some time that the cluster population shows no clear correlation between metallicity and age; indeed the oldest open clusters are as metal-rich as the youngest (Friel 1995; Salaris et al. 2004; among others). We have plotted on the left panel of Figure 7.5, the Figure 4 of Friel et al. (2002) showing that this holds true for their homogeneous sample of 39 old clusters. In the right panel, Figure 10 of Chen et al. (2003) is plotted for their 118 open cluster sample with a least square fit marked with a solid line. Both panels show the mean [Fe/H] for each cluster, after removing the effect of a linear abundance gradient of -0.06 dex $kpc^{-1}$, as a function of age.

The gradient with age found by Chen et al. is strongly dependent on very few points as already mentioned by the authors. Friel et al. (2002) results show that the oldest clusters are also among the most metal-rich for their position in the Galaxy. Our set of clusters, marked as solid diamonds in the right panel, can be seen at $-0.21$ for NGC 2548 (0.4 Gyr), $-0.23$ for NGC 1817 (1.1 Gyr) and $+0.05$ for the oldest in our set NGC 2682 (4.2 Gyr), all corrected for the radial gradient. Our values agree well with the lack of a general age-metallicity correlation.

Ortolani et al. (2005) discussed the possibility of a dip in the age distribution of old open clusters (see their Figure 11), where clusters in the range 3 to 9 Gyr are still rare. Old open clusters are located at highest Galactic latitude, and, in fact, we only know a few clusters located distant from the centre of the Galaxy (Villanova et al. 2005). The existence of an age-metallicity gradient as well as discussions about possible peaks or dips should be carefully considered as it is quite probable that more clusters remain to be discovered in this age range (as noted by Carraro et al. 2005). The completeness of the sample and homogeneity of the ages are crucial issues which have to be carefully taken into account before drawing conclusions on the star formation history of the Galactic disk using old open clusters.

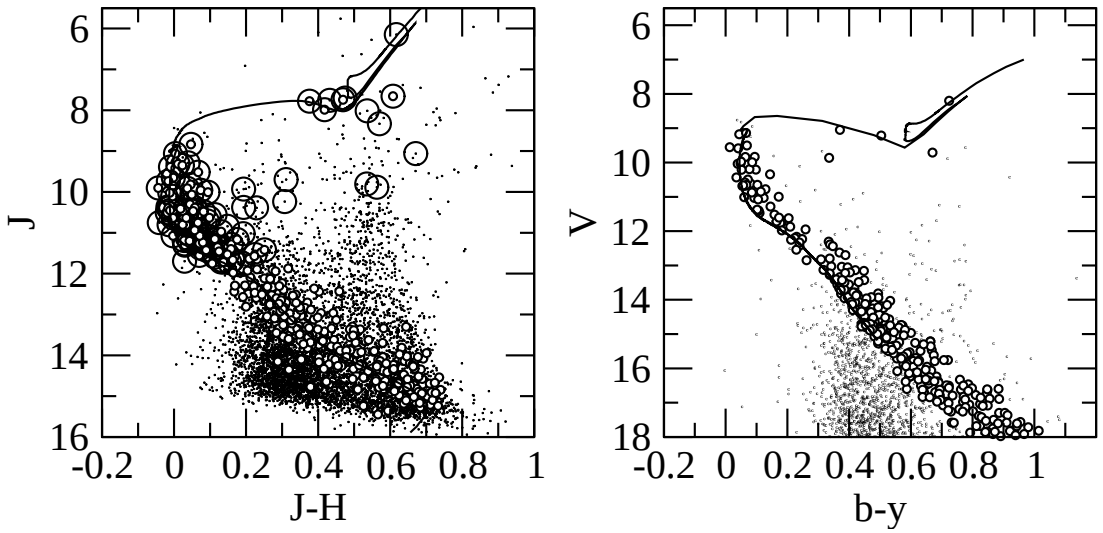


Figure 7.6: NGC 2548 IR colour-magnitude diagram from 2MASS (left) in the area of $1\overset{\circ}{.}5 \times 1\overset{\circ}{.}5$ covered by the astrometry and the optical one (right) in the smaller area covered by our photometry ($34' \times 34'$). Small empty circles are our candidate members, big circles (marked only on the left panel) are the astrometric members.

## 7.3 Luminosity functions

A reliable determination of the cluster luminosity function[1] requires a good segregation of cluster and field stars and the most complete sample possible. The cluster/field segregation has been carefully studied in previous chapters, with photometric and astrometric criteria. On the other hand, the data incompleteness has a strong dependence on the crowding/density of stars in the field and the stellar magnitude such that the data is less complete in crowded regions and towards faint magnitudes. But although our fields are not crowded, our mosaic photometry from different telescopes and instruments makes it difficult to estimate the completeness magnitude of the sample, apart from giving the photometric limit of the different areas.

The area coverage is reasonably wide for comprising most of the cluster in NGC 1817 and NGC 2682 (see Figures 3.1 and 6.1, respectively). On the contrary,

[1]Sections 7.3 to 7.5 are based on: Balaguer–Núñez L., Jordi C. and Gilmore G., 2005b, Proceedings of the 13th Joint European and National Astronomical Meeting. Granada, 13-17 September 2004.

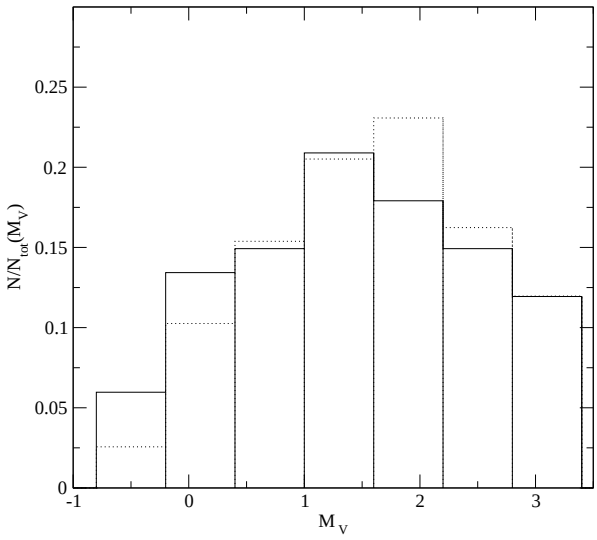


Figure 7.7: Luminosity function of NGC 2548, up to the limiting magnitude of the astrometry. Solid lines are from our photometry, dotted lines are from 2MASS with our astrometric selection. The difference in the normalised functions is within the uncertainties.

in the case of NGC 2548, our photometry clearly does not cover all the cluster, as it extends up to a few arcmins more than the half-sample radius at 14.38′. To check for the effect due to this incompleteness in the spatial coverage on the luminosity function derived from our optical data, we compare it with that obtained with the IR data from the 2MASS Catalogue[2] (Skrutskie et al. 1997). The Two Micron All Sky Survey (2MASS) has a depth (survey completeness limit of $J = 15.8$, $H = 15.1$, $K = 14.3$) and homogeneity crucial to properly take into account the stellar background contribution to the cluster as well as to check for possible spatial limitations. Figure 7.6 shows the colour-magnitude diagram for the IR colours from 2MASS applying our astrometric segregation and the one yielded by our optical photometry with a smaller coverage in sky area.

The luminosity function of NGC 2548, up to the limiting magnitude of the astrometry, is shown in Figure 7.7. We have applied our astrometric segregation to the 2MASS data and rejected a few stars with photometry clearly not compatible with the sequence of the cluster in $J$ vs $J - H$. Solid lines are from our photometry, dotted lines are from 2MASS (transformed to $M_V$ using Pietrinferni et al. 2004) with

[2] http://www.ipac.caltech.edu/2mass/releases/second/

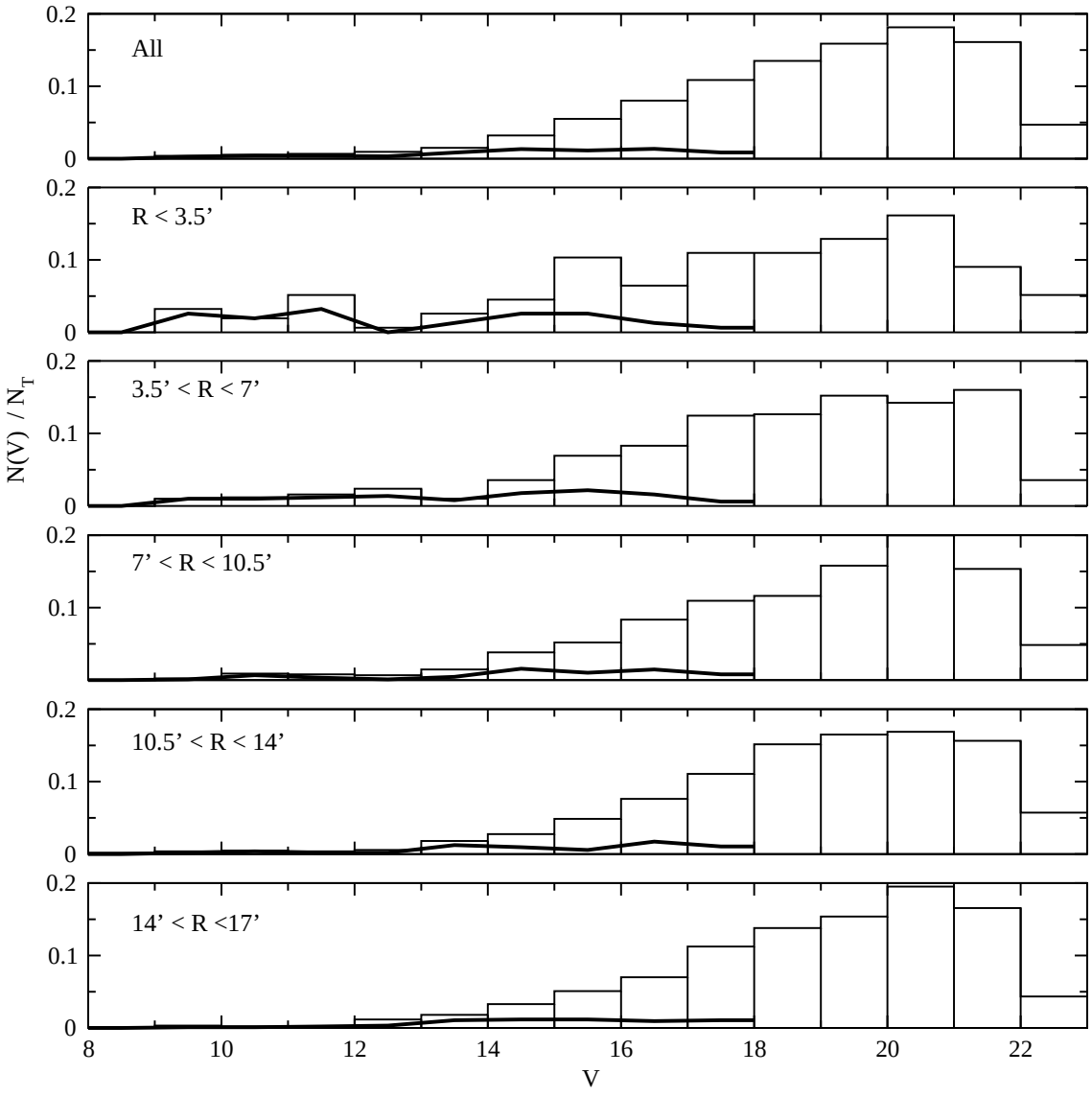


Figure 7.8: Observational total luminosity function from our photometry in annuli at increasingly large radii from the NGC 2548 cluster centre (histograms), normalised to the number of stars per annuli. The thick solid lines are the actual cluster member distribution.

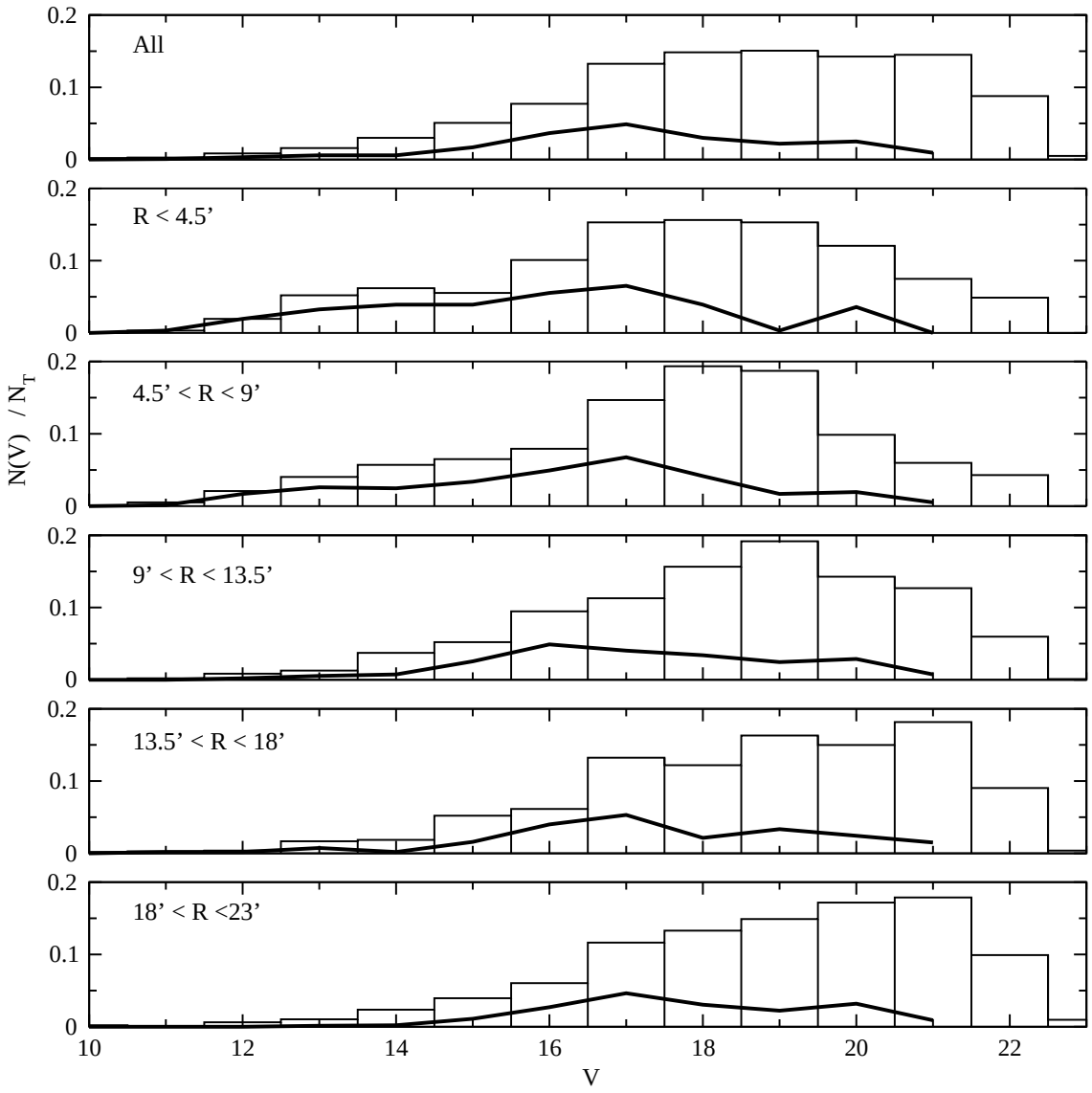


Figure 7.9: Same as Figure 7.8 for NGC 1817.

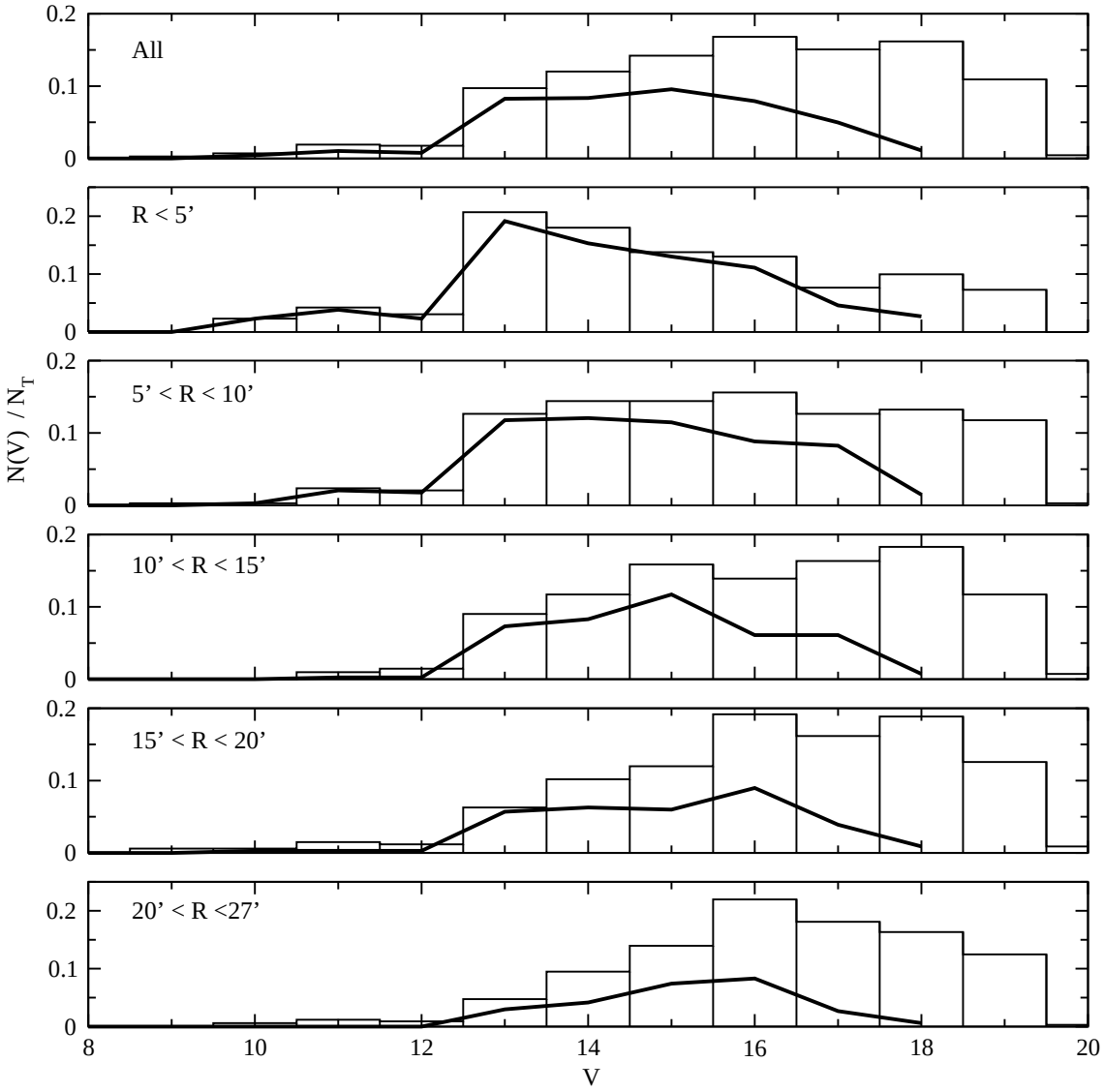


Figure 7.10: Same as Figure 7.8 for NGC 2682 (M 67).

our astrometric selection as seen in Figure 7.6. The difference in the normalised luminosity functions is within the uncertainties. Spatial bias does not seem to affect significantly our results. Moreover, the higher proportion of bright member stars compared to faint ones in our photometric sample can give us a hint of mass segregation.

From our selection of members, to derive the luminosity functions is straightforward. We have plotted the luminosity functions of the three clusters in Figures 7.8, 7.9 and 7.10. The luminosity functions are drawn for the total area and for five diferent annuli at increasingly large radii from the cluster centre. The histograms show all the stars in the area covered, normalised to the total number of stars per annuli, while the cluster member stars, also normalised, are indicated in thick solid lines. Our selection of member stars has the limiting magnitudes of $V = 18$ for NGC 2548, 21 for NGC 1817 and 18 for NGC 2682.

From these luminosity functions we can compare the richness of the clusters against the total number of stars. We observe that NGC 2682 is a very rich cluster, while NGC 2548 is rather poor.

The effect of mass segregation is already visible in the three clusters. Mass segregation will be better studied analysing the radial profiles of the different populations in Section 7.5.1.

## 7.4 Mass functions

The mass-luminosity relation from the appropriate isochrones computed by Pietrinferni et al.[3] (2004) has been used to derive individual masses of the cluster members needed to calculate the total mass of the cluster as well as the mass function. The mass functions of the three clusters are shown in Figure 7.11.

The mass function for stars is commonly written in the form of a Salpeter (1955) power law: $\mathrm{d}N(M) \propto M^{-\alpha}\mathrm{d}M$. We calculate the mass function slopes with a power law fitting in the common range 0.8 - 1.3 $M_{\odot}$ for the three clusters. The common upper limit is marked by the most evolved cluster NGC 2682. The low limit extends to the mass function region where the functional behaviour can no

[3] http://www.te.astro.it/BASTI/index.php

longer be considered as a power law, as can be seen in Figure 7.11. This change of behaviour may be due to the combination of our limited spatial coverage and the dynamical evolution and mass segregation effects due to the energy equipartition. These effects (see Section 7.5) produce that a fraction of low-mass stars will be beyond the central cluster region homogeneously covered by our mosaic photometry. Thus, to be on the safe side, we fixed the low limit for the calculation of the mass function slope at 0.8 $M_{\odot}$. This way we found a slope of $\alpha = 2.4 \pm 0.5$ for NGC 2548, and for NGC 1817 we obtain a slope of $\alpha = 2.7 \pm 0.5$, while for NGC 2682 we found a slope of $\alpha = 1.7 \pm 0.2$.

The values derived here for the slopes of NGC 2548 and NGC 1817, are in agreement, within the error, with the Scalo (1998) value $\alpha = 2.7 \pm 0.5$. While NGC 2682 results in a lower value of the slope in better agreement with the Scalo (1986) value of $2.00 \pm 0.18$ for field stars, the Salpeter (1955) value $\alpha = 2.35$ also for field stars or the value of $\alpha = 2.40 \pm 0.13$ from Phelps & Janes (1993) for young open clusters. The Francic (1989) value of $1.97 \pm 0.17$, found for six clusters is also well in accordance, while the value he found for M 67 is a rather unrealistic result of $-2.39 \pm 0.42$, in disagreement probably due to his smaller mass range, and it was not included in his composite mass function. Comparing these determinations is difficult because, beside the different samples and methods used, the result can depend on the mass interval used in each case. A summary of the different values of $\alpha$ and the corresponding mass interval is given in Table 7.3 for clarity.

Besides, in the study by Kroupa (2002) of the multi-part power law IMF, updated from Kroupa et al. (1993), a value of 2.3 (for stars more massive than 1 $M_{\odot}$) increased to 2.7 when correcting for unresolved binary systems. A significant percentage of binary or multiple stars in each cluster would lead us to underestimate the mass function slope. In other words, the determined mass function slopes are lower limits, because we have assumed that all stars detected are single stars. It is not straightforward to correct the observed mass functions for the presence of binaries, in particular since the binary fraction as a function of brightness is difficult to determine.

Fan et al. (1996) give a value of $1.93 \pm 0.66$ for the slope of NGC 2682 for stars with massses between 0.8 and 1.2 $M_{\odot}$ that agrees well with our result. Bonatto & Bica (2003) give a higher value of 2.41 for the central region and a 2.17 for the halo. Other dynamically evolved open clusters agree well with our value for NGC 2682.

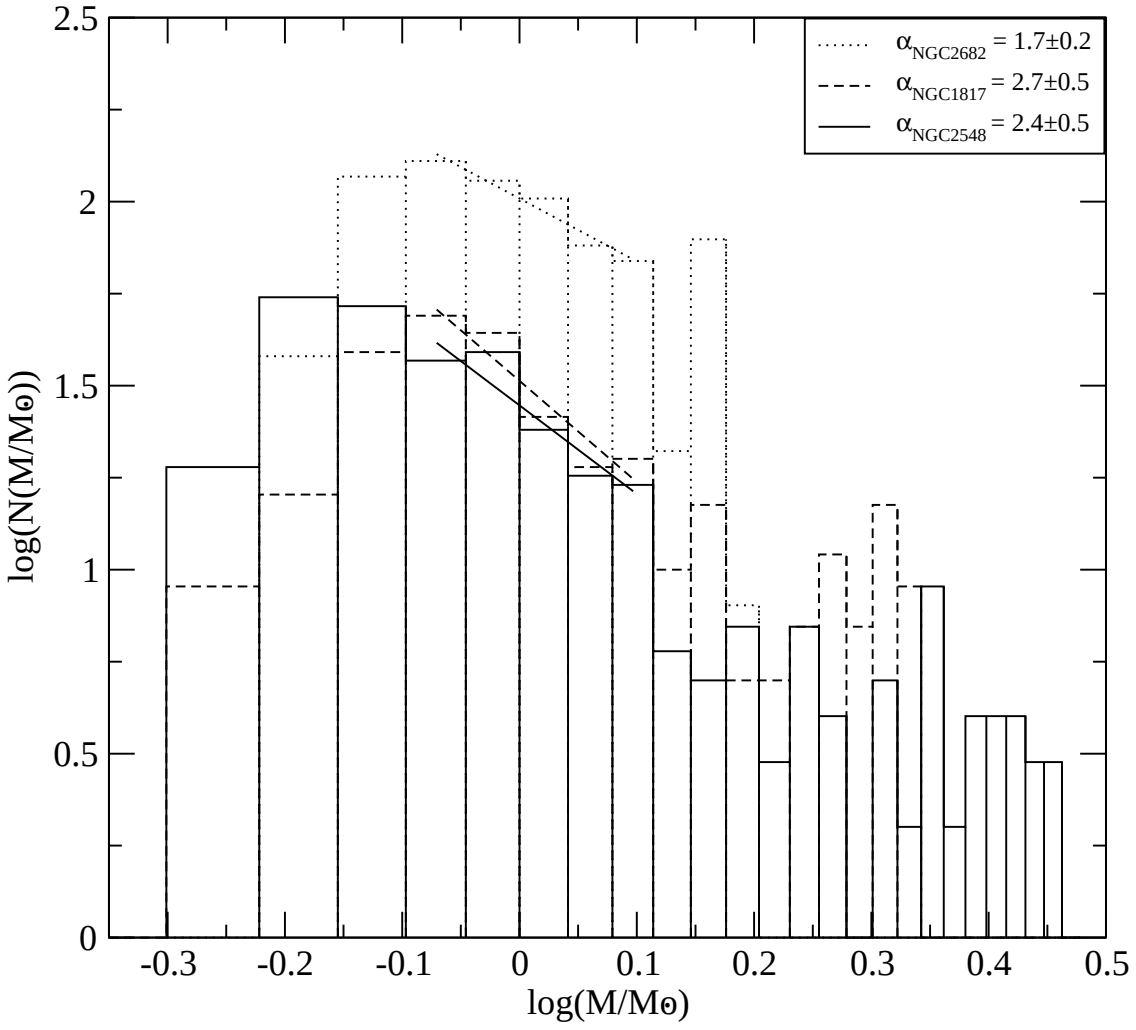


Figure 7.11: Mass functions of the three clusters NGC 2682 (M 67), NGC 1817 and NGC 2548 (M 48). The slopes of the power law fitting in the mass range between 0.8 and 1.3 $M_{\odot}$ are also indicated.

Table 7.3: Comparison of the mass function slopes from different authors.

| | $\alpha$ | Mass range ($M_\odot$) |
|---|---|---|
| Scalo (1998) | 2.7±0.5 | 1-10 |
| Salpeter (1955) | 2.35 | 0.4-10 |
| Phelps & Janes (1993) | 2.40±0.13 | 1.4-7.9 |
| Scalo (1986) | 2.00±0.18 | 0.8-18 |
| Francic (1989) | 1.97±0.17 | 1.1-2.5 |
| Kroupa (2002) | 2.3±0.3 | $< 1$ |
| (binary corrected) | 2.7±0.3 | |

Berkeley 99 with an age of 3.2 Gyr has a slope of 2.4±0.6 (Sagar & Griffiths 1998) and NGC 188 with solar metallicity and an age of 7 Gyr has a value of 1.9±0.7 (Bonatto et al. 2005).

McClure et al. (1986) and Pryor et al. (1986) suggested that the slope of the mass function is related to the metallicity of the cluster. They proposed that the observed dependence of mass function slopes on metallicity reflects, at least in part, properties of the IMF with which the clusters formed. Later, Djorgovski et al. (1993) demostrated that the MF slopes are determined not only by the metallicity but also by the location in the Galaxy. They showed that the clusters closer to the Galactic centre have flatter mass functions. At a given Galactocentric distance, clusters with a smaller distance from the Galactic plane have flatter mass functions, and at a given position, cluster with lower metallicities have steeper mass functions. Other authors interpreted the dependence on position as the effect of tidal shocks. Piotto & Zoccali (1999) suggested that the flattening of mass function slopes might be related to the cluster's dynamical evolution. From $N$-body simulations, Baumgardt & Makino (2003) predicted that the slope of mass functions of clusters should decrease constantly as the clusters evolve, because of the evaporation of low-mass members.

Our three clusters agree qualitatively with the just described relation of the mass function slopes with metallicity, $R_{\rm a}$, $z_{\rm max}$ and age. With NGC 1817 having the steepest slope (2.7) and being the farthest ($R_{\rm a}$ = 10.92 kpc, $z_{\rm max}$ = 424.8 pc) and with the lowest metallicity ([Fe/H] =−0.34) of the three. NGC 2548 following in slope (2.4) has an $R_{\rm a}$ = 9.56 kpc and a $z_{\rm max}$ = 239.4 pc, and with [Fe/H] =−0.24.

Table 7.4: Comparison of the mass function slopes with metallicity, distance, age and diameter parameters of the clusters under study.

| | $\alpha$ | [Fe/H] | $R_{\rm a}$ | $z_{\rm max}$ | Age | $D$ |
|---|---|---|---|---|---|---|
| | | dex | kpc | pc | Gyr | pc |
| NGC 1817 | 2.7±0.5 | −0.34±0.26 | 10.92±0.40 | 424.8±12.7 | 1.1±0.1 | 12 |
| NGC 2548 | 2.4±0.5 | −0.24±0.27 | 9.56±0.07 | 239.4±2.3 | 0.4±0.1 | 6 |
| NGC 2682 | 1.7±0.2 | +0.01±0.14 | 9.13±0.01 | 461.4±4.6 | 4.2±0.2 | 5.2 |

On the other hand, NGC 2682 has a flatter slope (1.7) as corresponds to a cluster closer to the Galactic centre with $R_{\rm a}$ = 9.13 kpc and $z_{\rm max}$ = 461.4 pc, and with [Fe/H] =+0.01 and being the oldest. Moreover, Burki (1977) computed the mass function for a set of very young clusters (1-20 Myr) and found that the slope varied with their size. He found that clusters with diameters less than 4 pc had larger slopes than those with diameters larger than 8 pc. Mackey & Gilmore (2003a) discuss the trend found in LMC clusters that the spread in core radius is an increasing function of cluster age. This trend could reflect physical evolution of clusters, with some clusters experiencing little or no core expansion, while others undergo large-scale expansion. Large core radii in globular clusters have been ascribed to accretion by the Galaxy of systems like the present-day satellites or to formation and evolution in low density regions (Mackey & Gilmore 2004; Wilkinson et al. 2003). Another explanation for generating a large core radii is the merger of a binary pair of clusters (see de Grijs et al. 2002, and references therein). A summary of all the cluster's information is given in Table 7.4 for clarity.

The differences in the present day mass function slopes are consistent with a combination of the metallicity dependence of the mass-luminosity relation, and with different dynamical evolution among clusters. The dynamical evolutionary effects have already affected the MF of the clusters under study, as they are all older than 100 Myr, which is a typical time-scale for dynamics to affect such stellar systems. Systematic changes with time away from the primordial mass function of a cluster are an unavoidable consequence of internal dynamical evolution: mass segregation, stellar merging, mass-dependent mass and star loss from the cluster (see Gilmore 2001 for a review). In any case, sampling and observational effects, together with the many contributions to Malmquist bias (Kroupa et al. 1993), dominate the available data. The range of slopes seen is consistent with the effects of dynamical evolutions

which are feasible, assuming a universal IMF.

## 7.5 Mass segregation

Mass segregation produces the accumulation towards the centre of the most massive stars (or binaries). Dynamical evolution, together with the effects of a tidal field, alters the cluster mass function as low-mass stars are stripped preferentially from the outer regions (Terlevich 1987). Galactic tidal stripping forces the cluster to adjust its structure and induces the contraction of the core. In some cases, this process can lead to a catastrophic collapse of the core. Mass segregation is observed at different degrees in the three clusters. This can be already seen in the luminosity functions derived in Section 7.3. Now, we will apply additional analysis to deepen into this subject.

### 7.5.1 Surface brightness profile

Following Mackey & Gilmore (2003a,b), we have calculated the surface brightness profiles of the three clusters. For each of them, several sets of circular annuli were constructed around the cluster centre. Each set has different annulus widths designed for sampling the different regions of the cluster: narrow ones for the most central regions and larger widths for the outer (less dense) regions. All the profiles were therefore extended to the maximum possible radii.

To calculate the surface brightness for a given annulus, we simply considered the flux of the member stars. For each set, the surface brightness $\mu_i$ of the $i$-th annulus is given by:

$$\mu_i = C - 2.5 \log(\frac{A_i}{\pi(b_i^2 - a_i^2)} \sum_{j=1}^{N_s} F_j) \tag{7.1}$$

where $b_i$ and $a_i$ are the outer and inner radii of the annulus respectively, $N_s$ is the number of stars in the annulus, and $F_j$ is the flux of the $j$-th star. The factor $A_i$ is the area correction for an annulus and must be determined when the annulus is constructed. To estimate the internal error $\sigma_i$ for an anulus we use the Poisson statistics.

The area correction $A_i$ for the $i$-th annulus is used simply to normalise the flux in the annulus to that for a full annulus. This is necessary because the shape of the mosaic photometry means that for all clusters, some annuli are not fully covered by our photometry. Since the flux through an annulus is directly related to the annulus area, variations in the fractions of annuli covered would cause artificial fluctuations in a surface brightness profile, and must therefore be accounted for. The area correction also takes into account the completitude limit of different areas of the mosaic having different limiting magnitudes. As the brightness profiles are divided in magnitude bins this correction can be easily performed.

We fit an empirical King model (King 1962) to the surface brightness profiles of our clusters:

$$\mu(r) = k \left\{ \frac{1}{[1 + (r/r_c)^2]^{1/2}} - \frac{1}{[1 + (r_t/r_c)^2]^{1/2}} \right\}^2 \tag{7.2}$$

where $r_t$ is the tidal radius of the cluster, and $r_c$ the core radius. Provided that $r_t >> r_c$, the core radius may be considered as the radius at which the surface brightness has dropped to half its central value. In implementing each fit, and following Mackey & Gilmore again, we develop a grid in the parameter space and chose the combination of parameters which minimises the weighted sum:

$$\chi^2 = \sum_{i=1}^{N_a} \left( \frac{\mu_i - \mu(r_c, r_t, k)}{\sigma_i} \right)^2 \tag{7.3}$$

where $\mu_i$ is the surface brightness of the $i$-th annulus, $\sigma_i$ is the error in this value, $N_a$ is the total number of annuli in the set in question and the other parameters are as defined in Equation 7.2. A refined mesh is then expanded about this parameter combination and the iteration continued until convergence. Convergence was reached typically within ten iterations.

For NGC 2548, to calculate the surface brightness profile we have divided the member stars in four bins, up to a maximum radius of $17'$, as can be seen in Figure 7.12 and summarised in Table 7.5. There are no blue stragglers detected in this cluster, and the number of red giants is too small to be treated as a separate sample. Thus, they are included in the brightest bin. As mentioned in Chapter 5, no information on binaries is available. We can observe how the most massive stars

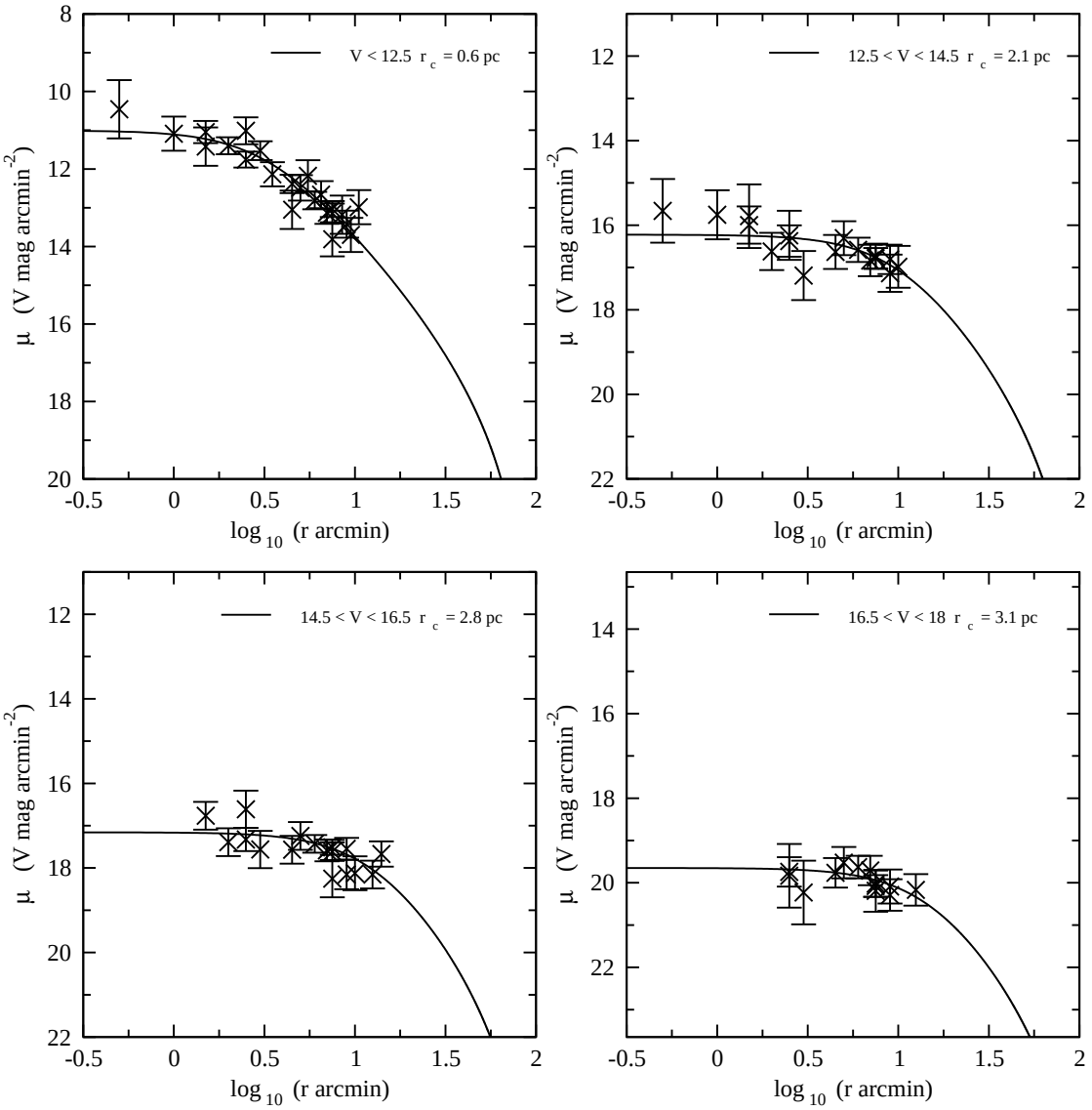


Figure 7.12: The surface brightness profiles of NGC 2548 (M 48). Blue stragglers have not been found in this cluster. The number of giants is too small to make a reliable fitting, so we study the profiles only in magnitude bins.

Table 7.5: Core radius of the different magnitude bins of the three clusters, ordered by size

| NGC 2548 | | NGC 1817 | | NGC 2682 | |
|---|---|---|---|---|---|
| Magnitude bin | $r_c$ | Magnitude bin | $r_c$ | Magnitude bin | $r_c$ |
| | | Blue Stragglers | $5.3'$ (2.8 pc) | $V < 13$ | $3.7'$ (1.0 pc) |
| | | Red Giant Binaries | $6.4'$ (3.4 pc) | Red Giants | $3.8'$ (1.0 pc) |
| $V < 12.5$ | $2.9'$ (0.6 pc) | $13.5 < V < 14.5$ | $7.2'$ (3.8 pc) | $13 < V < 14$ | $4.0'$ (1.1 pc) |
| $12.5 < V < 14.5$ | $10.1'$ (2.1 pc) | $V < 13.5$ | $9.3'$ (4.9 pc) | Binaries | $4.7'$ (1.2 pc) |
| | | Single Red Giants | $10.1'$ (5.3 pc) | Blue Stragglers | $6.9'$ (1.8 pc) |
| $14.5 < V < 16.5$ | $13.5'$ (2.8 pc) | $14.5 < V < 16.5$ | $18.9'$ (9.9 pc) | $14 < V < 15$ | $7.1'$ (1.9 pc) |
| $16.5 < V < 18$ | $14.8'$ (3.1 pc) | $16.5 < V < 18$ | $49.1'$ (25.7 pc) | $15 < V < 16$ | $7.2'$ (1.9 pc) |
| | | $18 < V < 21$ | $35.8'$ (18.7 pc) | $16 < V < 17$ | $8.6'$ (2.3 pc) |
| | | | | $17 < V < 18$ | $12.6'$ (3.3 pc) |

are more concentrated. In spite of being the cluster with the smallest area coverage of our photometric study, and also the closest one, the half-sample radius calculated in Section 5.3.4 of 3.0 pc is well covered by our study. We can already see the mass segregation effect in the area studied.

For NGC 1817, we have divided the member stars in five magnitude bins plus the blue stragglers (BS) bin and the red giants divided into single and binaries bins, as can be seen in Figure 7.13 and Table 7.5. The annuli are taken up to a maximum radius of $23'$. In spite of the possible contamination by the field among faint stars (where astrometric segregation is not available), we can clearly observe that more massive stars are more centrally concentrated. Contrary to what Raboud & Mermilliod (1994) found in other clusters older than 0.6 Gyr, mass segregation is present between single and binary red giants, as already pointed by Mermilliod et al. (2003). Blue stragglers are the most centrally concentrated stars, even more than the red giant binaries.

For NGC 2682, we have also divided the member stars in six magnitude bins plus spectroscopic binaries, blue stragglers and red giants bins as can be seen in Figure 7.14 and Table 7.5. The annuli are taken up to a maximum radius of $27'$. We can observe that more massive stars are more centrally concentrated. Red giants and stars with $V < 13$ are the most concentrated stars, and binaries are even more concentrated than blue stragglers. Raboud & Mermilliod (1994) confirmed this higher concentration of the binaries in M 67 found in Mathieu & Latham (1986), and a possible sub-concentration among the binaries related to their mass ratio.

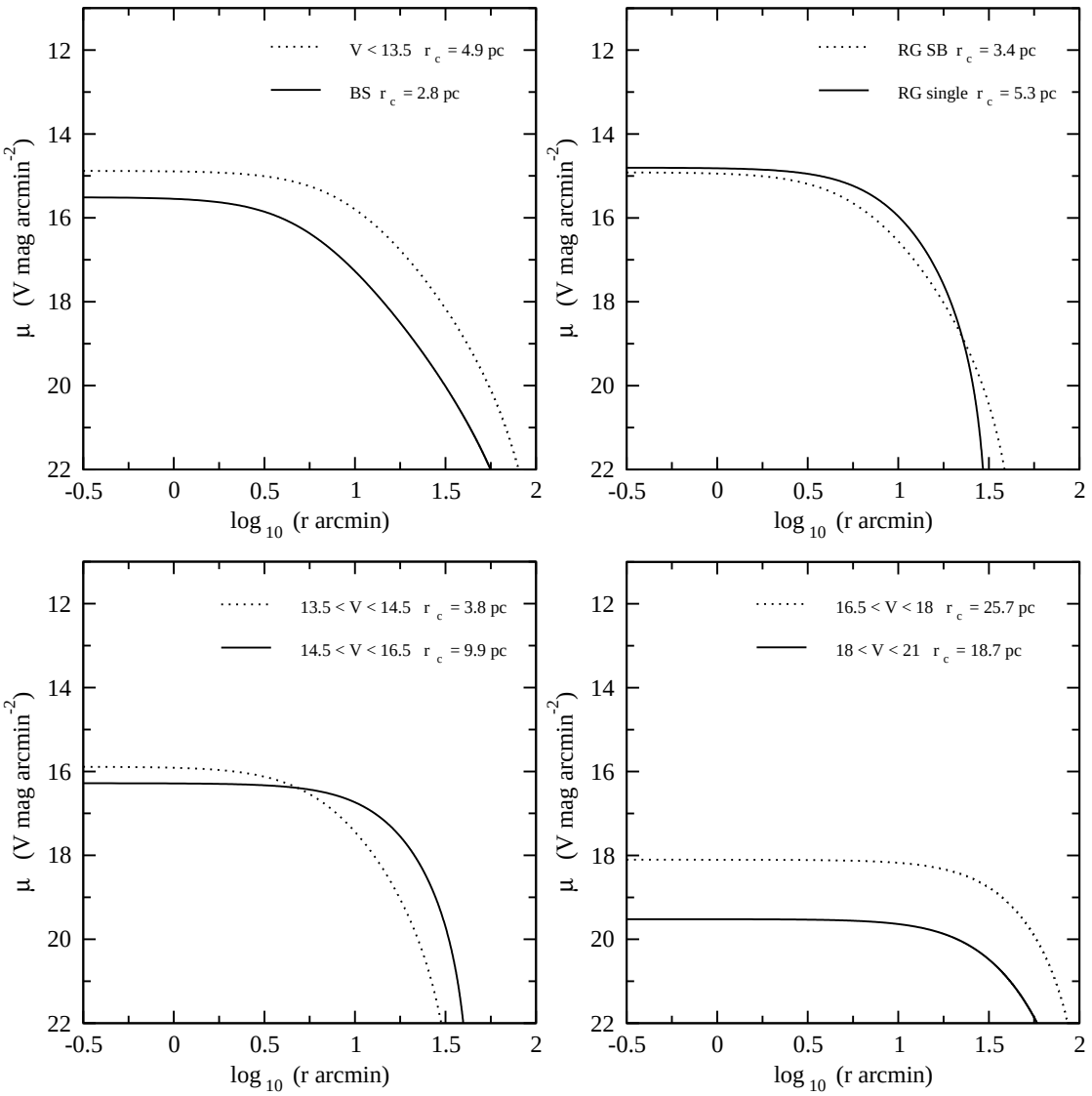


Figure 7.13: The surface brightness profiles of NGC 1817. The blue stragglers (BS), single red giants (RG), red giant spectroscopic binaries (RG SB) and five bins with different magnitudes are separated. The different points are not plotted for clarity.

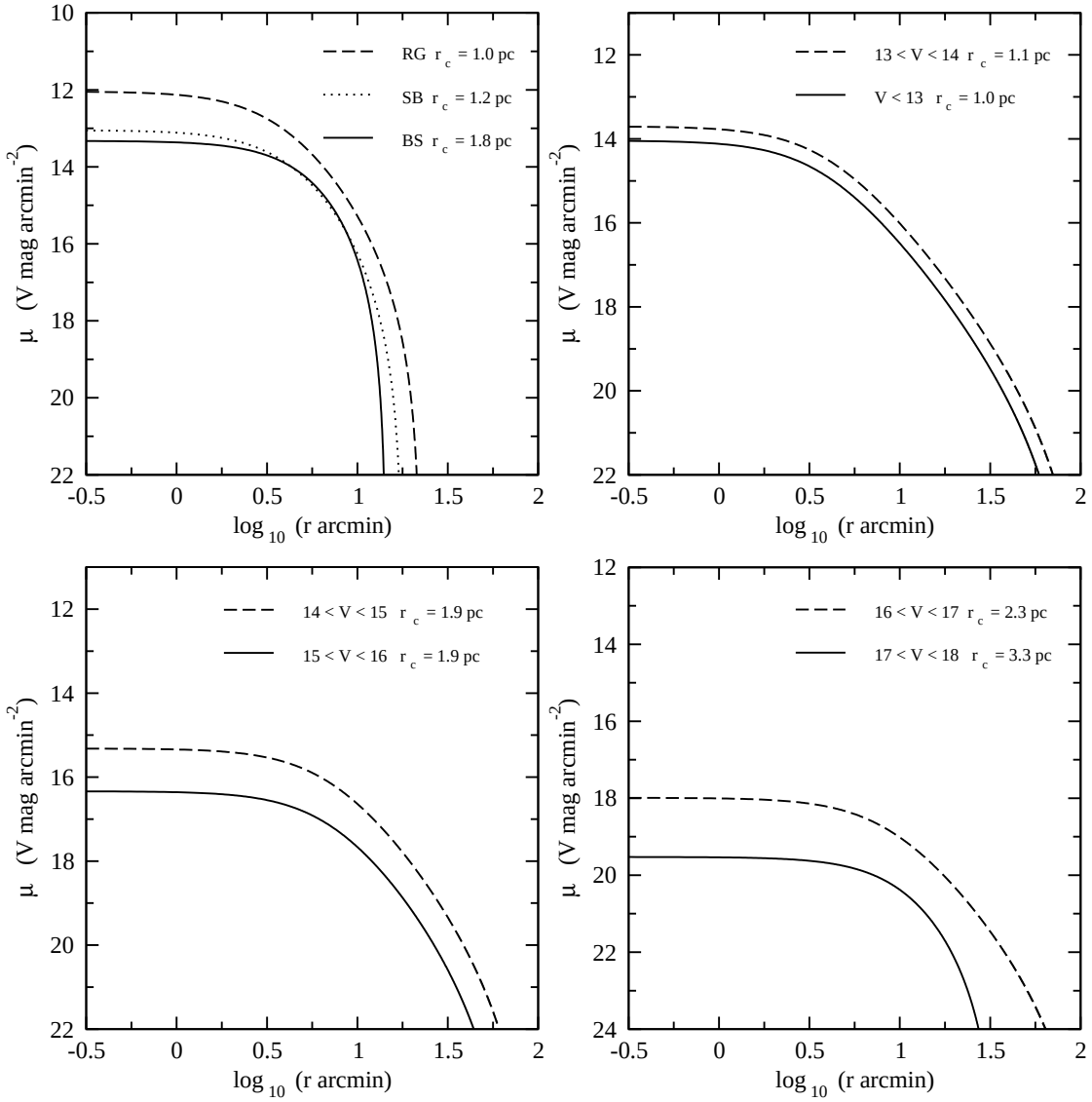


Figure 7.14: The surface brightness profiles of NGC 2682 (M 67). The blue stragglers (BS), red giants (RG), spectroscopic binaries (SB) and six bins with different magnitudes are separated. The different points are not plotted for clarity.

We calculate the median relaxation time $t_{\rm rh}$ (in the form of Mackey & Gilmore 2003a, but see also, for example, Spitzer & Hart 1971; Binney & Tremaine 1987) for the clusters using,

$$t_{\rm rh} = \frac{6.5 \times 10^8}{\ln(0.4N)} (\frac{r_{\rm h} h^{3/2}}{m}) (\frac{M_{\rm tot}}{10^5})^{1/2} \tag{7.4}$$

where $N$ is the total number of member stars, $m$ is the mass of the particular heavy star which sinks in time (we take $m = 2$ M$_\odot$), $M_{\rm tot}$ is the total mass of the cluster and $r_{\rm h}$ is the half-sample radius.

NGC 2682 has a $t_{\rm rh} = 2.8{\times}10^7$ yr, much shorter than its age of 4.2 Gyr. The cluster is indeed expected to be well relaxed as around 150 relaxation times had passed. All the bright and massive stars are strongly concentrated as shown by our results. Mathieu & Latham (1986) gives a relaxation time of $1{\times}10^8$ yr, in any case short relative to the cluster age.

NGC 1817 has a $t_{\rm rh} = 8.98{\times}10^7$ yr while its age is 1.1 Gyr, that means around 10 relaxation times. The red giants spectroscopic binaries (RG SB) are strongly concentrated while single RG do not show the same concentration. The cluster appear to be well relaxed.

NGC 2548 has a $t_{\rm rh} = 2.1{\times}10^7$ yr with an age of only 400 Myr, that is around 20 relaxation times. Our results show evidence of existing mass segregation although with a lower degree than in the other two clusters. Taking into account that the total mass estimates are low limits of the true total mass, and knowing that a greater fraction of members is not accounted for in the case of NGC 2548, thus we should take this relaxation time as a lower limit. Mass segregation should be still in process in this cluster.

Additionally, Baumgardt (1998) has shown that it is the tidal radius at the perigalacticon —the innermost point— of an eccentric orbit what determines the dissolution of a star cluster. During the perigalactic passages in an eccentric orbit, a lot of stars are stripped away suffering a stronger tidal field. The main effect of a stronger tidal field is to drive the cluster evolution at a higher rate. NGC 1817 and NGC 2682 are not only the oldest clusters in our study but also the ones with highest eccentricity in their orbits and smaller perigalactic radii $R_P$, i.e., suffering a stronger tidal field. In the case of NGC 1817, this could explain its evolutionary state and level of mass segregation. There is not a simple relation between mass-segregation

and age, nor with the number of red giants.

The local relaxation time gives us the time-scale in which heavy stars sink in the potential well. Stars far out in the halo of a cluster take longer to sink into the core. In clusters with longer relaxation times, this could be a good observational test of the formation mechanism of blue stragglers: any blue stragglers formed from primordial binaries in the cluster halo should still be in the halo. This will be thoroughly discussed in next Section.

### 7.5.2 Blue Stragglers

Blue stragglers are cluster main-sequence stars that seem to have stayed on the main sequence for a time exceeding that expected from standard stellar evolution theory for their mass. They lie above and blueward of the turn-off in the cluster colour-magnitude diagram, they appear to linger or *straggle* in their evolutionary process, hence the name "blue straggler" (see Stryker 1993). Many studies have discussed the issue during the last 50 years since it was discovered in the globular cluster M 3 by Sandage (1953).

Two viable mechanisms for blue stragglers formation have been suggested (see Bailyn 1995 and references therein):

- primordial blue stragglers formed via mass transfer between, or the merger of, two stars in a primordial binary (where primordial refers to binaries created when the cluster formed)
- dynamical blue stragglers formed via collisions in regions of very high stellar density. This class can be further subdivided into those produced by direct collisions (those created as collisions harden primordial binaries until they merge) and those resulting when binaries are produced in a collision and merge later.

Many authors have noted that those made from collisions in dense clusters may have different characteristics from those resulting from binary mergers of primordial binaries in sparse clusters. Blue stragglers made from collisions should be systematically brighter than those made from mergers of collisional binaries (Bailyn &

Pinsonneault 1995). Hurley et al. (2001) using a complete $N$-body code for cluster dynamics, have modelled the scenarios involving binary evolution dividing the merging process in three cases, depending on the evolutionary state and the mass of the two stars. They conclude that this evolution of primordial binaries can account for the single blue stragglers and the short- and long-period binary blue stragglers. But it is unable to explain binary BSs in eccentric orbits and/or wide binaries, or with masses greater than twice the cluster turn-off mass (McCrea 1964), nor it can account for the large number of observed blue stragglers. The influence of the cluster environment can effectively double the number of blue stragglers produced, leading to a better agreement with observations. Scenarios where the dynamical interactions in a cluster evironment become important are needed. As already pointed by Leonard (1996) several mechanisms have been at work to have created a blue straggler population with the observed diversity in binary properties. Moreover, in the case of NGC 2682 (M 67), there is no one unique mechanism able to explain the production of all the blue stragglers.

Blue stragglers are highly visible tracers of binary populations in addition to providing an opportunity to learn how interactions in binary systems affect stellar evolution. The study of blue stragglers provides insights into the dynamical interaction and evolution of individual stars but also of clusters as a whole. Star clusters evolve dynamically through interactions between cluster stars. Binaries are thought to play a fundamental role in core collapse: binary-binary collisions could be effective in delaying the collapse of the core. In this case, while the core tries to collapse, most of the binaries in the central regions will be destroyed by close encounters, and the survivors will become tightly bound, producing an overabundance of blue stragglers as noted for globular clusters.

The Hubble Space Telescope has allowed the inspection of the cores of globular clusters revealing that blue stragglers are more concentrated than the normal stars of the same luminosity (Piotto et al. 2004). Piotto et al. also found a strong anticorrelation of the blue stragglers frequency with cluster total luminosity and with the stellar collision rate. Contrary to what one would expect, clusters with higher total mass and clusters with higher collision probability have a much smaller fraction of blue stragglers. Those observations were then explained by Davies et al. (2004), who argued that the number of blue stragglers produced via collisions tends to increase with cluster mass, whilst the ones produced via primordial binaries decrease with increasing cluster mass. The evolution of primordial binaries is affected

by the cluster environment, and, in particular, it is accelerated in clusters where the encounter probability is higher. Clusters with high encounter probability have favoured the formation of blue stragglers from primordial binaries in the past. Now these binaries have already evolved and cannot form blue stragglers any more, explaining the observed relative absence in high mass clusters. It also agrees with the relatively larger fraction of blue stragglers among field stars (e.g. Carney et al. 2005), where the even lower-density environment makes the evolution by encounters slower than in any cluster, allowing them to produce blue stragglers for a more extended time interval. Mass segregation has also an effect on the location of the blue stragglers, inferring that, at least in some clusters, a large fraction of any primordial blue straggler population is still to be found in the cluster haloes.

The binary properties of blue stragglers in several clusters should be measured and compared with the binary properties of main-sequence, subgiant and giant stars in the same clusters to better determine its origin and mechanisms of evolution. Open clusters, on the other hand, are ideal laboratories to study blue stragglers as they are less affected by crowding problems, nor are so vulnerable to stellar encounters as globulars do. And have the advantage of the membership segregation thus having a better known origin than field blue stragglers.

Before analysing our sample of blue stragglers, we can perform a further check on the reliability of the selection, drawing the $V$ vs $(u-y)$ diagram (see Figure 7.15). Since red giants are faint in $UV$, the photometric blends, which mimic blue stragglers in visible colour-magnitude diagrams are less problematic (see for example Sabbi et al. 2004). This helps to clean our selection of blue stragglers.

Many studies have been done in M 67 and its rich and varied population of binaries and blue stragglers. Having between a 30-50% of binaries and, at least, 23 blue stragglers, it is an ideal object to test the different theories. It has a super-blue straggler (S0977), a single star with a mass of $\sim 3$ $M_{\odot}$, more than twice the cluster turn-off mass. And another one (S1082) that is a triple system with one of the stars being a blue straggler by itself (van den Berg et al. 2001; Sandquist et al. 2003). Three interacting W UMa systems, variables, X-ray sources... all pointing to a very rich and complex evolution. Of all its blue stragglers only 2 are slightly farther than its half-sample radius (at $10.71'$ and $10.81'$) and two other farther (at $15.56'$ and $17.83'$). NGC 2682 had time to reach core collapse (according to Binney & Tremaine 1987 core collapse occurs at 12 to 19 median relaxation times), and all its bright stars

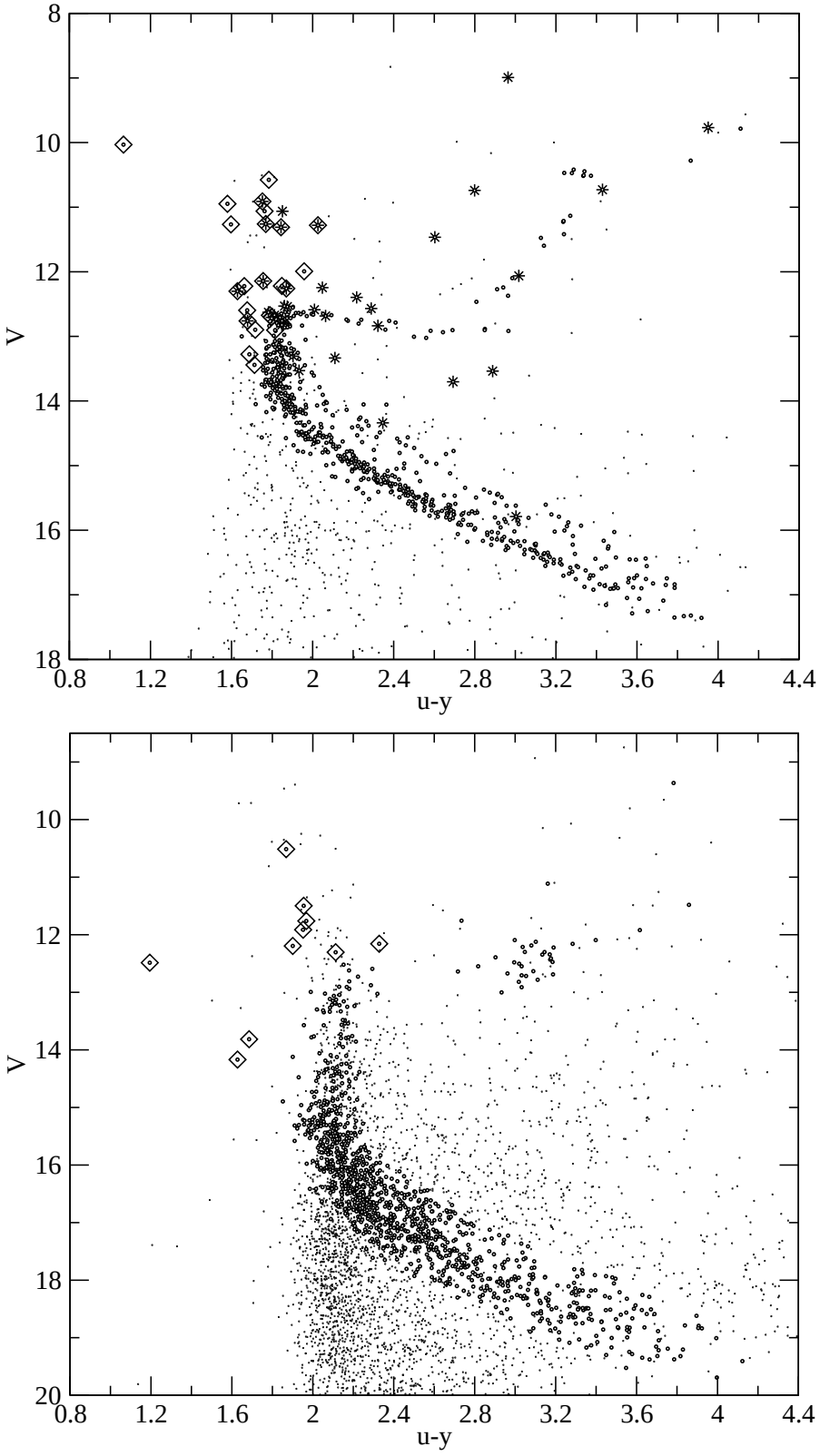


Figure 7.15: $V$ vs $(u-y)$ for NGC 2682 (upper plot) and NGC 1817 (lower plot). Blue stragglers marked as diamonds, binaries as stars.

remain in the centre with its red giants and binaries even more concentrated than the blue stragglers. Through a complete $N$-body modelling of the BSs in M 67, Hurley et al. (2001) concluded that half of them have primordial progenitors whilst half have been formed via dynamical interactions. Mathieu & Latham (1986) show that the central concentration of the binaries and the blue stragglers is consistent with them being more massive objects in a relaxed cluster. They fit the spatial distribution of all the stars in the cluster with a multimass equipartition King model with a 2 $M_\odot$ component to model binaries and blue stragglers. They find the BS and SB similarly concentrated, but their sample of BS is restricted to only 11 of the brightest. In our sample, the $r_c$ of BSs is similar to that of stars in the main sequence region between $14 < V < 15$ ($\sim 1$ $M_\odot$).

The blue straggler data is not sufficiently numerous to determine accurately the masses of these stars via dynamical models. Indeed, there is no reason to believe that all of them have the same mass, in any case. In fact, we can plot the appropriate isochrones (see Figure 7.16) from the set of Pietrinferni et al. (2004) with the corresponding metallicities, reddening and distance modulus in the colour-magnitude diagram for both clusters. For NGC 1817 (left plot), in the isochrone of 0.9 Gyr, the mass of the stars at the turn-off is $M_{\rm TO} = 1.92$ $M_\odot$; then, going towards blue colour and younger ages: age 0.5 Gyr ($M_{\rm TO} = 2.35$ $M_\odot$), age 0.3 Gyr ($M_{\rm TO}$ =2.83 $M_\odot$), age 0.2 Gyr ($M_{\rm TO} = 3.30$ $M_\odot$). For NGC 2682 (M 67), we have plotted the isochrones from 2.5 Gyr ($M_{\rm TO} = 1.46$ $M_\odot$), 1.8 Gyr, 1.2 Gyr, 1.0 Gyr, 0.7, 0.5 and 0.4 Gyr ($M_{\rm TO} = 2.70$ $M_\odot$). The reported isochrones encompass the whole distribution of BSs, thus constraining the range of masses covered by the BS to 1.9 $M_\odot \leq M_{\rm BS} \leq 3.3$ $M_\odot$ for NGC 1817 and to 1.5 $M_\odot \leq M_{\rm BS} \leq 2.7$ $M_\odot$ for NGC 2682. Blue stragglers with $M_{\rm BS} \leq 1.5$ $M_\odot$, i.e. formed by the merging of low mass main-sequence stars, are still hidden in the main sequence. There are some BS that cannot lie on the main sequence of any reasonable isochrone, but which can be well fit by the sub-giant branch sequences. These stars have evolved to the thinning hydrogen burning shell phase and are rapidly moving to the base of the RGB, i.e., they are yellow stragglers (YS), and also some candidates to be evolved blue straggler (E-BS), i.e, a BS in its helium-burning phase (see Bellazzini et al. 2002 and references therein).

Given the finite lifetime of blue stragglers, the present blue straggler population in the richest clusters could be lower than in very sparse clusters. NGC 1817 is a sparse cluster with a high number of blue stragglers. Unfortunately, we do not have

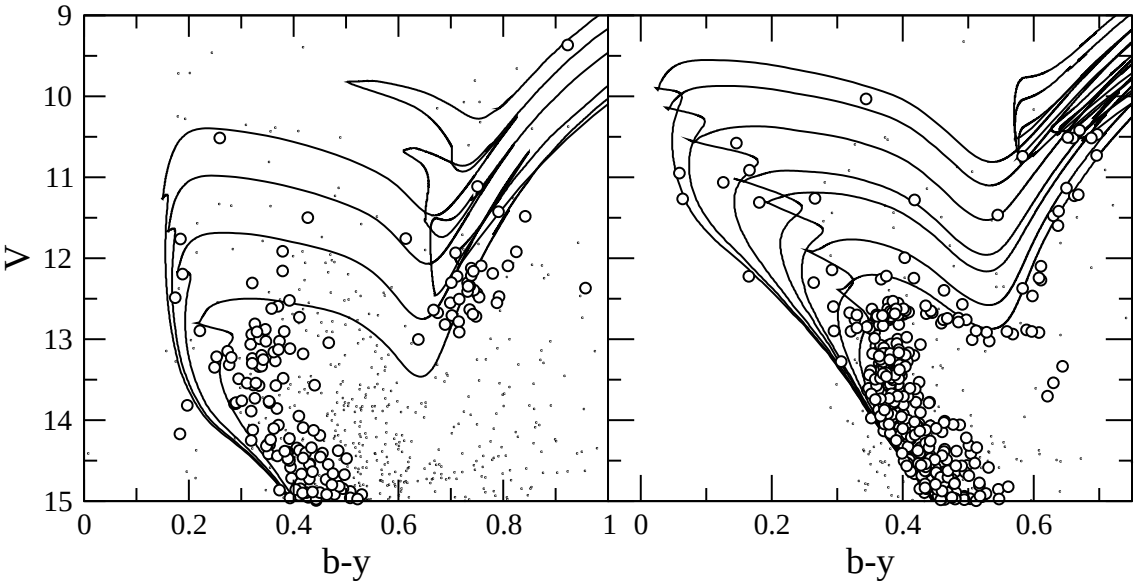


Figure 7.16: Isochrones from Pietrinferni et al. 2004 from left to right: ages 0.9, 0.5, 0.3, 0.2 Gyr for NGC 1817 (left plot) and 2.5, 1.8, 1.2, 1.0, 0.7, 0.5, 0.4 Gyr for NGC 2682 (right plot).

spectral information of those 11 BS, but a high number of binaries is found among red giants (Mermilliod et al. 2003). The blue stragglers are more concentrated than the red single giants (Figure 7.13) and this suggests that collisions are destroying giants and creating blue stragglers. NGC 1817, having a longer relaxation time, shows a distribution of BS very concentrated with a $r_c = 2.8$ pc comparable to that of the RG SB but still keeping three blue stragglers far out in the halo, (farther than its half-sample radius, at $14.21'$ and at $32.78'$ and $33.55'$ from the centre), pointing towards a primordial origin. At the same time, NGC 1817 has lower central density and bigger core radii than the other clusters under study. All of that can make us think of its peculiar orbit as a factor tightly linked to its dynamical evolution.

Bellazzini et al. (2002) studying two fields (one internal to the half-light radius and one external) of NGC 288, with deep HST photometry, found a similar central concentration of blue stragglers in spite of being a loose globular cluster. They also added more evidence for the formation of BSs via mass transfer/coalescence of primordial binary systems being as efficient as collisional mechanisms in the most favorable crowded environments. This argued in favour of a primordial origin in low stellar density environments, if a sufficient reservoir of primordial binaries is available. Having a 25.6% of binaries (Mermilliod et al. 2003) among the red giants

in NGC 1817 a primordial origin sounds very likely. Hurley & Shara (2002) from $N$-body simulations using GRAPE-6 arrived to the conclusion that although the possibility of any particular star becoming a blue straggler as a result of a dynamical encounter is quite random, once a star does become a blue straggler and, hence, one of the most massive stars in the cluster, subsequent interactions are almost unavoidable. NGC 1817 can be the perfect example of this behaviour.

## 7.6 Gaps in the Main Sequence

Gaps in the main sequence have been observed and debated for a long time [4]. In the Hyades, de Bruijne et al. (2000) confirmed the reality of two gaps near $B-V \sim 0.38$ and $B-V \sim 0.48$ ($T_{\rm eff} \sim 6400$ K). Evidence for the existence of gaps among field stars has also been debated Newberg & Yanny (1998), and recently Kovtyukh et al. (2004) showed a new gap among field stars in the effective temperature range 5560 to 5610 K.

### 7.6.1 Method

The characteristics of our photometry and member selection procedure allow us to pursue the search for gaps in the main sequence for all the clusters included in this project. To check the reliability of the results, we apply the same gap search to the Pleiades (M 45) and the Hyades, two well-known clusters in which gaps have been previously reported (de Bruijne et al. 2000, Belikov et al. 1998, and specially their Figures 1 and 3, respectively).

We estimate effective temperatures for our selection of candidate members following a new approach (Ribas et al. 2003; Masana et al. 2005) based on fitting observed IR photometry with accurately calibrated synthetic photometry. We use our values of $V$ magnitude and the 2MASS values for $J$, $H$, and $K$ magnitudes. The process requires metallicity and surface gravity data that we compute from our Strömgren photometry as explained in previous chapters. The method is restricted to the temperature interval from 4000 K to 8000 K, with quoted uncertainties of

[4] This section is based on: Balaguer-Núñez L., Jordi C., & Galadí-Enríquez D., 2005, A&A 437, 457

0.5-1.3%. The upper temperature limit is due to the increased dependence of the results on the accuracy of $\log g$, while the lower limit is related to the decreasing performance of the models because of molecular bands. Masana et al. (2005) show that, in this range, the procedure is essentially insensitive to the adopted value of [Fe/H] and $\log g$: uncertainties of 0.3 dex in metallicity and 0.5 dex in gravity induce $T_{\rm eff}$ deviations inferior to 0.5%. The number of member stars from our selection of clusters that also have 2MASS photometry in the range of temperatures under study is of 269 stars for NGC 2548, 307 stars for NGC 1817 and 588 stars for NGC 2682. For Pleiades we obtain 225 member stars and for Hyades 76.

After getting the $T_{\rm eff}$ values, we proceeded to the gap search following a method analogous to that proposed by Rachford & Canterna (2000). A simple $\chi^2$ test with one degree of freedom is used to evaluate the significance of any candidate gap. To do this, we take a candidate gap of width $W_{\rm in}$ and we compute the number of stars within it, $N_{\rm in}$. This number is compared with the stars located on both sides of the gap. We take two bins of equal width, $W_{\rm out}$, at the sides of the candidate gap, and we count the stars inside them, $n_{\rm out}$. Then, $n_{\rm out}$ is scaled to the size of the gap to give $N_{\rm out} = W_{\rm in} n_{\rm out}/(2W_{\rm out})$ and this quantity is compared to $N_{\rm in}$ to get the $\chi^2$ value. To limit the effect of small number statistics, and again following Rachford & Canterna (2000), the computation is done only when at least five stars are present on each side of the gap, which guarantees that $n_{\rm out} \geq 10$.

We performed this calculation for a grid of gap widths 75 K $< W_{\rm in} <$ 500 K, at intervals of 25 K, and placing the gap centres every 1 K over the intersection of the temperature range covered by the method with the range covered by the photometry. To prevent edge effects, intervals of 300 K were avoided at the extremes of the intersection.

After several trials, we chose $W_{\rm out} = 100$ K for our photometry, but the Pleiades and Hyades required $W_{\rm out} = 200$ K, due to the smaller size of the photometric sample. It is important to note that widening $W_{\rm out}$ can alter the relative value of $\chi^2$ and its associated probability, but with little effect on the significance of the gap centre position or width.

Having computed $\chi^2$ for the whole range of gap centres and sizes, we select the local maxima of the resulting table. We observe that changes in $W_{\rm in}$ do not make gaps appear or disappear, but only affect their significance. All significant gaps have probability values higher than 0.99.

Table 7.6: Gaps in temperature empirically detected in the main sequence of open clusters.

| Cluster | Age | [Fe/H] | Centre | Width | Centre | Width | Centre | Width | Centre | Width |
|---|---|---|---|---|---|---|---|---|---|---|
| | Gyr | dex | K | K | K | K | K | K | K | K |
| Pleiades (M 45) | 0.1 | -0.03 | 7377 | 300 | 6821 | 325 | 5577 | 275 | 4845 | 275 |
| NGC 2548 (M 48) | 0.4 | -0.24 | 7099 | 475 | 6305 | 425 | 5465 | 350 | 4785 | 350 |
| Hyades | 0.7 | 0.15 | 7006 | 475 | 6427 | 250 | 5452 | 225 | 4972 | 275 |
| NGC 1817 | 1.1 | -0.34 | 7323 | 175 | 6674 | 350 | 5701 | 300 | - | - |
| NGC 2682 (M 67) | 4.2 | 0.01 | - | - | - | - | 5593 | 125 | 5017 | 200 |

### 7.6.2 Results

Table 7.6 gives the centres and widths ($W_{\rm in}$) for the significant gaps in the temperature range studied. The two well-known Böhm-Vitense gaps at 7200 K and 6600 K are clearly detected in Hyades and also Pleiades, which serves as a check of the reliability of the method. Both gaps are significant in the whole sample of clusters analysed, with the exception of M 67, due to the much higher age of this stellar system (the main sequence is so evolved that the corresponding effective temperature range is no longer populated).

The gap recently reported by Kovtyukh et al. (2004) in field stars at 5560-5610 K, and already suspected in the Hyades (de Bruijne et al. 2000), stands out not only in the Hyades, but also in the other clusters surveyed. In the case of M 67, Fan et al. (1996) also raised the possible existence of this gap placed around 1 $M_{\odot}$.

The reliability of the new gap detected around $T_{\rm eff} \sim 4900$ K is stressed by its appereance in all the clusters under study with the only exception of NGC 1817. The reason is that, in this case with the cluster being at 1800 pc, our photometry does not reach stars colder than 5000 K.

Even though we know that some amount of field contamination is present in our candidate member selection, the significance of the four gaps in our photometric data is outstanding. If an even more reliable member selection would be possible, this could make the gaps even more evident in our data.

The position and width of the gaps is compared with the age and metallicity of the clusters in Figure 7.17. No clear trend can be drawn from this comparison.

Table 7.7: Orientative and approximate characterisation of the mean loci of the gaps detected.

| $< T_{\rm eff} >$ (K) | $\sigma_{<T_{\rm eff}>}$ (K) | $B$–$V$ | Spec. | Mass ($M_{\odot}$) |
|---|---|---|---|---|
| 7200 | 180 | ∼0.30 | F0 | ∼1.6 |
| 6600 | 230 | ∼0.40 | F2-F5 | ∼1.3 |
| 5600 | 100 | ∼0.70 | G5-G8 | ∼0.80 |
| 4900 | 110 | ∼0.90 | K2 | ∼0.75 |

However, metallicity effects could be masked due to the uncertainties in the metallicity determinations used for NGC 2548, NGC 1817 and NGC 2682 (M 67) that are of the order of 0.2 dex.

Independently of the physical explanation for the existence of these gaps, there is no reason, in principle, to expect them to appear at the same positions and with similar sizes in all the clusters. There can be a complex dependency on metallicity and other parameters. However, the clusters studied show some regularity that allows to distinguish, as mentioned, four independent gaps. Even though we know that this kind of average may lack physical meaning, we give a table with mean, approximate parameters that characterise the loci of the four gaps (Table 7.7). The colour indexes and masses are taken from standard relations (Schmidt-Kaler 1982) and assume solar metallicity.

Several theoretical explanations have been proposed for the three hotter gaps (see the references already given). Most but probably not all, are related to rotation and convection. However, theoretical and/or empirical references to the fourth, colder gap are lacking. Spectroscopy could confirm or reject the reality of this gap whose significance is similar to that of the others, on the basis of our photometric data.

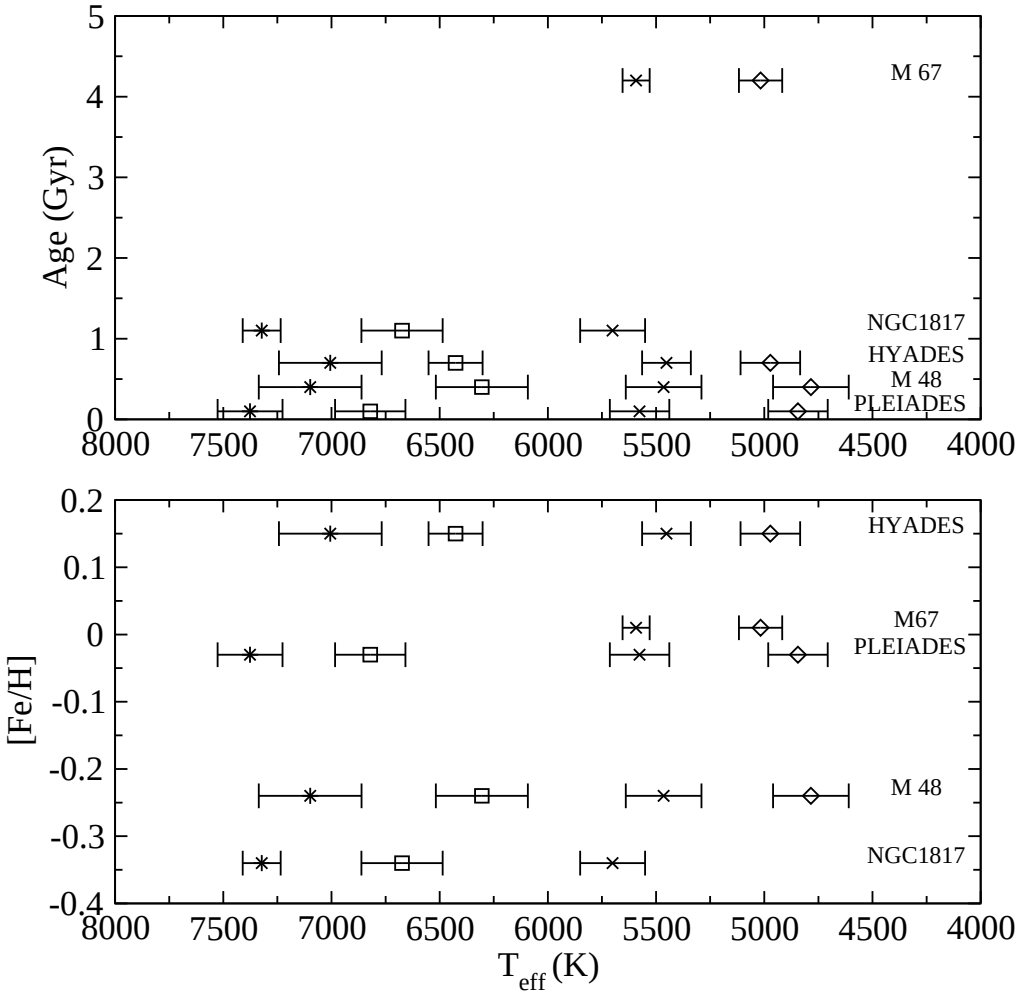


Figure 7.17: Gaps in temperature vs age (upper panel) and metallicity (lower panel).